

1 **Observations of Aerosol-Vapor Pressure Deficit-Evaporative Fraction coupling over India**

2

3 Chandan Sarangi^{1,2,7*}, Tirthankar Chakraborty^{3,4}, Sachchidanand Tripathi^{1,3*}, Mithun Krishnan¹,
4 Ross Morrison⁵, Jonathan Evans⁵, Lina Mercado ^{5,6}

6 Affiliations:

7 ¹ Department of Civil engineering, Indian Institute of Technology, Kanpur, Kanpur, India

8 ² Department of Civil engineering, Indian Institute of Technology, Madras, Chennai, India

9 ³ Center for Environmental Science and Engineering, Indian Institute of Technology, Kanpur

10 ⁴ School of the Environment, Yale University

11 ⁵ UK Centre for Ecology & Hydrology, Wallingford, UK

12 ⁶ Department of Geography, University of Exeter, UK

13 ⁷ Laboratory of Atmospheric and Climate Sciences, Indian Institute of Technology, Madras,
14 Chennai, India

16 * Corresponding authors: snt@iitk.ac.in and chandansarangi@iitm.ac.in

18 **Abstract**

19
20 North India is a densely populated subtropical region with heavy aerosol loading (**mean Aerosol**
21 **Optical Depth or AOD ~ 0.7**), frequent heatwaves and strong atmosphere-biosphere coupling,
22 making it ideal for studying the impacts of aerosols and temperature variation on latent heat flux
23 (LH) and evaporative fraction (EF). Here, using in situ observations during the onset of the
24 summer monsoon over a semi-natural grassland site in this region, we confirm that strong co-
25 variability exists among aerosols, LH, air temperature (T_{air}) and vapor pressure deficit (VPD).
26 Since the surface evapotranspiration is strongly controlled by both physical (available energy and
27 moisture demand) and physiological (canopy and aerodynamic resistance) factors, we separately
28 analyze our data for different combinations of aerosols and T_{air} /VPD changes. We find that
29 aerosol loading and **warmer** conditions both reduces SH. Further, we find that an increase in
30 atmospheric VPD, tends to decrease the gross primary production (GPP) and thus LH, most
31 likely as a response to stomatal closure of the dominant grasses at this location. In contrast, under

Formatted: Line spacing: 1.5 lines

Formatted: Superscript

Formatted: Superscript

Formatted: Line spacing: 1.5 lines

Formatted: No underline

Formatted: Font colour: Text 1

Formatted: Font colour: Text 1

Deleted: ¶

Formatted: No underline

Deleted: heatwave

35 heavy aerosol loading, LH is enhanced partly due to the physiological control exerted by the
36 diffuse radiation fertilization effect (thus increasing EF). Moreover, LH and EF **increases** with
37 aerosol loading even under heatwave conditions, indicating a decoupling of plant's response to
38 VPD enhancement (stomatal closure) in presence of high aerosol conditions. **Our results**
39 **encourage detailed in situ experiments and mechanistic modelling of AOD-VPD-EF coupling for**
40 **better understanding of Indian monsoon dynamics and crop vulnerability in a heat stressed and**
41 **heavily polluted future India.**

Deleted: are positively associated

Deleted: With heat-stress, VPD and aerosols expected to increase in future India,

Deleted: o

Deleted: warrant

Deleted: in-depth analysis of aerosol

Deleted: plant-temperature-EF continuum

Deleted: and its impact on Indian monsoon dynamics and crop vulnerability

43 **Highlights:**

- 44 1. A rigorous analysis of Aerosol-EF-VPD coupling using collocated direct observations is
- 45 presented
- 46 2. Increased aerosol loading enhances Evaporative Fraction by decreasing sensible heat and
- 47 increasing latent heat.
- 48 3. Aerosols modulate the response of vegetation to changes in VPD under heatwave conditions
- 49

50 **Keywords:** Grassland, Aerosol loading, eddy covariance, evaporative fraction, physiological
51 response, diffuse radiation, Indo Gangetic Plains, heatwave, sensible heat, latent heat, Bowen
52 ratio.

Deleted: ¶

53 **Introduction:**

54 The surface energy balance represents the balance between the net radiation (NR) flux at
55 the Earth's surface and the partitioning of NR into latent heat (LH), sensible heat (SH) and
56 ground heat (GH) fluxes [Wang and Dickinson, 2012]. While the dominant partitioning of
57 energy as SH enhances the near-surface air temperature, the LH flux cools the surface and
58 increases the moisture content of the boundary layer. Thus, perturbations to the partitioning of
59 the outgoing turbulent energy fluxes from the land surface modify the near surface
60 micrometeorology. One way of representing this partitioning is the evaporative fraction
61 ($EF=LH/(SH+LH)$), or the proportion of the total available energy (NR-GH) available at the
62 surface released via vegetation **evapo**transpiration and soil evaporation. Earlier studies have
63 established that the EF can be modulated by a range of factors, including vapor pressure deficit

Deleted: incoming shortwave and longwave

Field Code Changed

Formatted: Font colour: Text 1

Deleted: Thus, enhancement in EF in a warmer environment also implicates the susceptibility of the vegetation present in a measured canopy/land cover to drought conditions. ¶

78 (VPD), soil moisture, canopy structure, atmospheric composition, solar radiation and stomatal
79 behaviour [Baldocchi, 1997; Wilson et al., 2002].

80 **The variability in** VPD, which describes the near surface moisture deficit for a given
81 temperature (difference between the saturated and ambient vapor pressure for atmospheric water)
82 is arguably the dominant nonlinear forcing on EF variability [Gu et al., 2006]. On one hand, an
83 increase in VPD leads to the partitioning of more of the available energy into LH to meet the
84 atmospheric moisture demand, part of the physical control on evapotranspiration [Penman, 1948;
85 Monteith et al., 1965]. On the other hand, high VPD also triggers partial closure of leaf stomata
86 in response to increased atmospheric dryness [Jones and Sutherland, 1991; Damour et al., 2010;
87 Medlyn et al., 2011]. This is part of the physiological control on ET, causing an increase in VPD
88 to actually decrease ET (and thus EF) [Rigden & Salvucci, 2017]. Moreover, the sign of VPD-
89 EF association could also change due to variations in confounding factors like ambient soil
90 moisture and diffuse/direct radiation [Gu et al., 2006]. More diffused radiation enhances plant
91 productivity [Mercado et al., 2009; Rap et al., 2018] and plant growth [Wang et al., 2018];
92 which, in turn, can increase LH and EF [Chakraborty et al., 2021; Davin et al., 2012; Wang et al.,
93 2008]. However, this association is also reported to have an optimum point beyond which plant
94 productivity declines with increasing **diffused** fraction **of radiation** [Knobl et al., 2008].

95 Small particles suspended in the atmosphere, i.e. atmospheric aerosols, can alter the
96 amount of shortwave and longwave radiation reaching the surface, through scattering and
97 absorption, thereby altering NR [Schwartz, 1996; Trenberth et al., 2009; Chakraborty and Lee,
98 2019]. This is commonly known as the aerosol direct radiative effect (ADRE) and is dependent
99 on aerosol size, composition and vertical distribution in the atmosphere [Forster et al., 2007;
100 Sarangi et al., 2016]. Global and regional scale modelling studies have reported that the ADRE
101 can greatly alter the surface fluxes and microclimate over land [Liu et al., 2014; Mallet et al.,
102 2009; Shen et al., 2020; Myhre et al., 2018]. Generally, the ADRE reduces NR, which results in
103 the reduction in the magnitude of SH and LH. But, loading of scattering aerosols from fossil fuel
104 combustion can also increase the diffuse fraction of solar radiation at the surface, which affects
105 the photosynthesis and LH or EF [Chameides et al., 1999; Matsui et al., 2008; Niyogi et al., 2004;
106 Wang et al., 2008; O'Sullivan et al., 2016; Wang et al., 2020]. This mechanism is generally
107 referred to as the **diffuse radiation induced aerosol** fertilization effect (ADFE). But, depending on

Formatted: Line spacing: 1.5 lines

Deleted: ET;

Formatted: Font colour: Text 1

Formatted: Font colour: Text 1

Field Code Changed

Field Code Changed

Formatted: Font colour: Text 1

Field Code Changed

Formatted: Font colour: Text 1

Formatted: Font colour: Text 1

Formatted: Font colour: Text 1

Formatted: Font colour: Text 1

Formatted: Font colour: Text 1

Formatted: Font colour: Text 1

Deleted: in the literature

Deleted: aerosol

111 the ecosystem, the positive association of ADFE on EF also gets saturated as ADRE becomes
112 larger than a threshold [Yue et al., 2017]. Further, Steiner et al., [2013] reported that warmer air
113 temperature are consistent with high aerosol optical depth (AOD) scenario over various in-situ
114 micrometeorological sites in USA, which can result in no clear association between AOD and
115 LH. Thus, how aerosol loading modulates the already complex VPD-EF association can depend
116 on the interplay between radiation, ADFE, aerosol amount and properties, background climate
117 and ecosystem phenology [Steiner et al., 2011].

Deleted: AOD

Formatted: Font colour: Text 1

118 Northern India is a global hot spot for atmospheric aerosols with AOD varying between 0.5 and
119 1.5, and high aerosol radiative efficiency values ($\sim 100 \text{ W/m}^2/\text{AOD}$) during pre-monsoon period
120 [Dey et al., 2011; Kumar et al., 2015; Dimitris et al., 2012; Sarangi et al., 2016; Srivastava et al.,
121 2011]. In addition, the region also experiences frequent high temperature days and heatwave
122 conditions, generally extending for 2-6 days during this period [Ratnam et al., 2016; Rohini et
123 al., 2016]. During heatwave conditions, the regional atmosphere is largely stagnant [Ratnam et
124 al., 2016], which can lead to greater air temperature by 5-10 K and magnifies the water vapour
125 demand by 2-3 times at weekly time scale. In addition to high air temperatures (T_{air}), high
126 aerosol loading during heatwaves have also been reported over Northern India [Dave et al., 2020;
127 Mondal et al., 2020] at this time of year. Moreover, the value of EF is typically greater than 0.5
128 over the Northern India during pre-monsoon period, indicating a potentially larger control of
129 VPD-LH linkages on surface energy partitioning [Bhat et al., 2019]. Steep variability in ambient
130 values of VPD (also AOD in some events) during heatwaves over Northern India provides us
131 with ideal conditions for investigating the associations between aerosol loading and VPD-EF
132 coupling.

Deleted: aerosol optical depth (AOD)

Field Code Changed

Field Code Changed

Formatted: Font colour: Text 1

Formatted: Font colour: Text 1

Formatted: Font colour: Text 1

133
134 Previous studies have suggested that aerosol loading can modulate the partitioning of surface
135 fluxes over Northern India [Urankar et al., 2012; Murthy et al., 2014; Latha et al., 2019; Gupta et
136 al., 2020]. However, these studies have been based on reanalysis products [Urankar et al 2012],
137 very limited measurements of SH only [Murthy et al., 2014] or estimated derived from remotely
138 sensed data [Latha et al., 2019] and therefore lack the fidelity that can be obtained from direct
139 observations of key processes. Better understanding of the aerosol-VPD-EF associations using
140 direct collocated observations is essential to understand present day conditions and potential

Field Code Changed

Formatted: Font colour: Text 1

Field Code Changed

Formatted: Font colour: Text 1

143 feedbacks that can modify future climate over this region of great hydro-climatic significance. In
144 this study, we have used co-located observations of surface energy balance, near-surface
145 micrometeorological variables and soil characteristics, together with aerosol properties (both
146 surface and columnar) at a sub-tropical site in northern India during the pre-monsoon season.
147 Analysis of case studies with AOD varying in phase or remaining constant with high VPD
148 (under heatwave conditions) are done to understand the underlying processes. Here, we will
149 present compelling evidence that changes in EF is directly (indirectly) proportional to aerosol
150 loading (VPD). More interestingly, we found that aerosol loading can decouple the observed
151 strong VPD-LH relationship under heatwave scenario which can have serious implications on
152 climate resilience of crops and vegetation. Below, the sections are organized to discuss the data
153 used, case studies selected and methodology, results, discussions and summary of this study.

154

155 **2. Observation site and data:**

156

157 Observations of SH, LH and net ecosystem CO₂ exchange (NEE) were obtained over a
158 semi-natural grassland site (Figure 1A) within the campus of the Indian Institute of Technology,
159 Kanpur (IITK; 26.5N, 80.3E, elevation 132 m above mean sea level) during the pre-monsoon
160 months (April-June) of 2016-2017. Energy flux data were collected by an eddy covariance
161 system installed at 5.28 m above the soil surface. This flux measurement site is part of an eddy
162 covariance network set up in India as part of the INCOMPASS project of the Indo-UK Monsoon
163 Programme [Chakraborty et al., 2019; Turner et al. 2019; Bhat et al., 2019]. The eddy covariance
164 system consists of a Windmaster sonic anemometer-thermometer (Gill Instruments Ltd.
165 Lymington, UK) and a LI7500 infrared gas analyzer (LI-COR Biosciences, Logan, Utah, USA).

166 ~~The fetch around the tower is a mixture of different C4 grasses, i.e. variants of Napier grass~~
167 ~~(~60-70%) and some common reed (Scientific family: Pennisetum purpureum and Phragmites-~~
168 ~~Saccharum-Imperata). Napier grasses are invasive and a perennial species and representative of~~
169 ~~grasslands in the region (Chakraborty et al., 2019; Holm et al., 1979).~~ The vegetation cover is
170 more than 90% of the fetch of the flux tower (Figure 1B) and the canopy height varied within 1-
171 1.5 m during our study periods. The soil is typical of the Gangetic Plains with silt, clay and sand
172 fractions of 80%, 15% and 5%, respectively (unpublished data). The site experiences a humid

Deleted: (EC)

Deleted: EC

Deleted: EC

Formatted: Font: Not Italic

Formatted: Font: Not Italic

Deleted: The fetch around the tower is a mixture of different C4 grasses that is representative of grasslands in the region.

178 subtropical climate. The range in daily AOD and T_{air} was 0.4-1.4 and 32-45 °C, respectively,
179 during the study period (Figure 1C).

Formatted: Font: Italic

180

181 The net radiation (NR; $W\ m^{-2}$) and its incoming and outgoing short- and longwave
182 components were measured using an NR01 net radiometer (Hukesflux, Delft, The Netherlands)
183 installed at 5 m above the surface. The surface temperature (T_{srf}) was calculated from the
184 measured outgoing longwave radiation following the Stefan–Boltzmann law assuming an
185 emissivity of 0.95 [Trenberth et al., 2009]. Ground heat fluxes (GH; $W\ m^{-2}$) were monitored at
186 0.03 m below the soil surface using two HFP01-SC self-calibrating soil heat flux plates
187 (Hukesflux, Delft, The Netherlands). Near surface air temperature (T_{air} ; °C) and relative humidity
188 (RH; %) were measured at a height of 4.5 m. Wind speed and wind direction were measured at
189 10 m above the soil surface using a WindSonic anemometer (Gill Instruments Ltd., Lymington,
190 UK). Volumetric soil water content (VWC; m^3 of water in m^3 of soil) and surface temperature
191 (T_{srf} ; °C) were measured using two pairs of digital TDT sensors (Acclima Inc., Meridian, Idaho,
192 USA) installed at 0.05 and 0.15 m below the soil surface. Standard data processing and quality
193 control routines were used to calculate surface fluxes as described in Morrison et al. 2019. Data
194 gap-filling and the partitioning of net ecosystem exchange into Gross Primary Production (GPP)
195 and total ecosystem respiration was performed using the R EddyProc package [Reichstein et al.,
196 2016; Reichstein et al., 2005]. Negative net ecosystem exchange during the daytime period
197 indicates that photosynthesis at our site dominates over soil and plant respiration (not shown).
198 Since water and carbon cycles in the plants are closely coupled [Collatz et al., 1991]; variations
199 in GPP are used as a proxy for plant transpiration in this study. More details on the flux, weather
200 and radiation tower measurements at IIT Kanpur can be found in Table S1 and Chakraborty et
201 al., 2019.

Deleted: Soil

Deleted: A

Deleted: NEE

Deleted: NEE

202

203 Version 2 instantaneous cloud screened (Level 1.5) half-hourly averages of Aerosol
204 Optical Depth (AOD) at 550 nm and Single Scattering Albedo (SSA), the ratio of scattering
205 efficiency to total extinction efficiency, at 440 nm obtained from the AErosol RObotic NETwork
206 (AERONET) station deployed in the IITK campus (Figure 1A) were used to quantify the aerosol
207 optical properties during our study period. Low and high SSA values indicate dominance of

Deleted: (

Deleted:)

214 absorbing and scattering aerosols in the column, respectively. Clear-sky short wave (0.25–4 μ m)
215 radiative transfer calculations, using the Santa Barbara discrete ordinates radiative transfer
216 Atmospheric Radiative Transfer Model (SBDART) [Ricchiuzzi et al., 1998], are used to estimate
217 the midday aerosol direct radiative forcing (ADRF) at surface and diffuse radiation reaching the
218 surface (diffuse_{frac}). Midday mean AOD and SSA for each day are prescribed to the model.
219 More details on radiative flux calculations using SBDART are mentioned in Supplementary
220 Information file. Finally, micro-pulse lidar backscatter images (Level 1.5) measured at the
221 collocated Micro-Pulse Lidar Network site [Campbell et al., 2002; Welton and Campbell, 2002]
222 are also used in this study, mainly to identify cloudy days. A day is termed as a cloudy day if
223 cloud patches are observed in Lidar profiles for more than 3 hours. More details on the aerosol
224 measurements can be found in supplementary information file.

Deleted: SW

Deleted: DISORT (

Deleted:)

Deleted: (MPLNET)

Field Code Changed

Formatted: Font colour: Text 1

Formatted: Font colour: Text 1

Deleted: MPLNET

226 3. Case studies and methodology:

227
228 In order to examine the impact of aerosols or VPD on EF, we need to carefully identify
229 periods where the variability of other confounding factors is negligible. As such, we identified
230 three weeks (marked in Figure 1C) for analysis, where daily variations in all these factors except
231 T_{air} /VPD and AOD is negligible. Figure 1C illustrates the occurrences of cloudy days, rainfall
232 and wildfire-affected periods during pre-monsoon months of 2016 and 2017. We have avoided
233 periods of cloud and rainfall occurrences since that would affect the surface and energy budget
234 much more than the ADFE. The daily mean VWC values are also shown for the period in Figure
235 1C. However, as shown in Figure 1C, it is rare to have a considerable time interval with only
236 variation in AOD values (and negligible variation in T_{air} /VPD). Eventually, three one-week
237 periods are carefully selected with different combinations of dominant weekly gradients in T_{air}
238 /VPD and AOD and analyzed to gain insights into ambient AOD-VPD-EF association. The first
239 week selected for analysis is between 2nd-9th June, 2016, which had high weekly gradient in
240 AOD but was accompanied by low variation in T_{air} /VPD (hereafter referred as High AOD-Low
241 T_{air} (HALT) case). The second week is during 10th-15th April, 2017, which witnessed large daily
242 increase in aerosol loading as well as T_{air} in phase throughout the week (hereafter referred to as
243 the High AOD-High T_{air} (HAHT) case). We also selected a third week during 10th-15th May,
244 2017, when high gradient in T_{air} was observed across the week, but negligible weekly gradient in

Deleted: The measurements at our site reflect land-atmosphere-energy balance continuum. Thus, in

Formatted: Indent: First line: 1.27 cm, Line spacing: 1.5 lines

Deleted:

Formatted: Font: (Default) Times New Roman, Not Italic

Formatted: Font: (Default) Times New Roman, Not Italic

253 AOD was present i.e the AOD values had large day to day variability through the week
 254 (hereafter referred to as the Low AOD- High T_{air} (LAHT) case). Interestingly, heatwave
 255 conditions were prevalent over North India during the HAHT and LAHT weeks, therefore, a
 256 wide range of VPD-AOD-EF variation can be sampled. Moreover, since there were no rainfall
 257 events during these three weeks, the variation in VWC was minor compared to large daily
 258 variations in T_{air} and AOD during our study periods. Further, the variations in the vegetation
 259 phenology, wind and boundary layer height are found to be negligible within each of these three
 260 weeks. Note that no week with low AOD and low VPD variations was observed during our study
 261 period.

Formatted: Font: (Default) Times New Roman, Not Italic

262 The simultaneous midday (1000-1500 LT) variability in AOD, VPD, EF and the other
 263 components of the surface radiative balance is analyzed across the HAHT and LAHT weeks to
 264 understand the impact of strong weekly gradients of AOD and VPD, respectively. Further, we
 265 analyse the weekly gradients in the observations during HAHT, and compare and contrast the
 266 same with the HAHT and LAHT cases to understand the combined effects of AOD and VPD.

Deleted: Hence, three different combinations of T_{air} /VPD and AOD is selected for analysis. The first week selected for analysis is between 2nd-9th June, 2016, which had large variation in AOD values is accompanied with insignificant daily variation in T_{air}/VPD (hereafter referred as High AOD-Low T_{air} (HALT) case). The second week is during 10th-15th April, 2017, which witnessed significant daily increase in aerosol loading as well as T_{air} (hereafter referred to as the High AOD-High T_{air} (HAHT) case). We also selected a third week during 10th-15th May, 2017, when daily variation of AOD is relatively low but the variation in T_{air} is high (hereafter referred to as the Low AOD- High T_{air} (LAHT) case). Interestingly, heatwave conditions were prevalent over North India during the HAHT and LAHT weeks, therefore, a wide range of VPD-AOD-EF variation can be sampled. It was also ensured that no rainfall happened during these three weeks so that the variation in VWC is minor compared to significant daily variations in T_{air} and AOD during our study periods. Further, the variations in the vegetation phenology, winds and boundary layer height are found to be minor within each of these three weeks. ¶

267 Moreover, to examine the impact of aerosol loading on VPD-EF associations under enhanced
 268 heat stress, we also calculated the daily midday bulk canopy resistances for both HAHT and
 269 LAHT cases by inverting the Penmann-Monteith equation as described below. We used observed
 270 values of available energy, VPD, T_{srf} derived from observed LW_{out}, psychrometric constant and
 271 slope of vapor pressure curve derived from observed surface pressure and T_{air} respectively, and
 272 aerodynamic resistance derived from the observed SH and near-surface temperature gradient.

Formatted: Font: Not Italic

273 The aerodynamic resistance to heat transfer (r_a) is calculated from the near-surface temperature
 274 gradient and the measured distance between the two (H), given by:

Deleted: The simultaneous midday (1000-1500 LT) variability in AOD, VPD, EF and the other components of the surface radiative balance is analyzed within the HAHT and LAHT cases to understand the susceptibility in various variables to changes in AOD and VPD variations, respectively. Further, we analyze the relative variability in HAHT, and compare and contrast the same with the HAHT and LAHT cases to understand the effect of combined effect of AOD and VPD variability.

Formatted: Line spacing: 1.5 lines

$$275 \quad r_a = \frac{-\rho C_p (T_{srf} - T_{air})}{H}$$

Deleted: the differences in canopy resistance and VPD association between HAHT and LAHT weeks is also calculated

Deleted: .

276 where T_{srf} is the surface temperature, calculated by inverting the Stefan-Boltzmann law assuming
 277 a unit surface emissivity (reasonable for vegetated surfaces), ρ is the air density, and C_p is the
 278 specific heat at constant pressure (1.005 x 10⁻³ MJ kg⁻¹ °C⁻¹).

Formatted: Font: Not Italic

Formatted: Font: Not Italic

Formatted: Font: Not Italic

Formatted: Font: Not Italic

Formatted: Font: Not Italic

Formatted: Font: Not Italic

308 Then, the canopy resistance (r_s) is calculated by inverting the Penman-Monteith approximation.

309 Thus:

$$310 r_s = \frac{\Delta(Rn - G) + \frac{\rho C_p VPD}{r_a} - \Delta}{\gamma - 1} r_a$$

Formatted: Font: Not Italic

311 where Δ is the slope of the water vapor saturation curve given by:

$$312 \Delta = \frac{4098[0.6108 \exp(\frac{17.27 T_a}{T_a + 237.3})]}{(T_a + 237.3)^2}$$

Formatted: Font: Not Italic

313 and γ is the psychrometric constant, calculated as:

$$314 \gamma = \frac{C_p P}{\epsilon \lambda}$$

Formatted: Font: Not Italic

315 where P is atmospheric pressure in kPa, λ is the latent heat of vaporization (2.45 MJ kg⁻¹), and ϵ
316 is the ratio of the molecular weight of water vapour to dry air (0.622).

Formatted: Font: Not Italic

Formatted: Font: Not Italic

317 4. Results:

Deleted: We calculated the daily midday bulk canopy resistances for both HAHT and LAHT cases by inverting the Penmann-Monteith equation using observed values of available energy, VPD, T_{surf} derived from observed LW_{surf} , psychrometric constant and slope of vapor pressure curve derived from observed surface pressure and T_{air} respectively, and aerodynamic resistance derived from the observed SH and near-surface temperature gradient. ¶

318

319 During the HALT period, midday AOD values decreased monotonically across the week from
320 ~1.1 on 2nd June, 2016 to ~0.6 on 9th June, 2016 (Figure 2A). The corresponding trend in SSA
321 values was negligible, but SSA values are ~0.92 indicating a predominance of scattering aerosols
322 (Figure 2A). Corresponding values of NR at surface increased monotonically by ~50 W/m²
323 during the same week (Figure 2D). The enhancement in midday NR with decreasing AOD is
324 strongly driven by the corresponding increase in midday incoming shortwave radiation (ISWR)
325 by ~100 W/m² (Figure 2D). In agreement, ADRF values at surface decreased by ~80 W/m² and
326 diffuse fraction of incoming radiation increased by ~0.10 with decrease in scattering aerosols
327 from 2nd June to 9th June, 2016 (Figures S1A and S1D). The daily trend in modelled ADRF (and
328 diffused fraction) values are consistent with the daily reduction trend of ISWR during HALT,
329 reinforcing the expectation that negative daily trend in ISWR and NR during HALT was
330 primarily by aerosol-induced radiative changes.

Deleted: daily

Formatted: Superscript

Deleted: period

Deleted: reduction

Deleted: ϵ_{frac}

Deleted: increase

331

344 During HAHT, the midday AOD values increased monotonically across the week from
 345 ~0.3 on 10th-11th April to ~0.8 on 14th-15th April (Figure 2B). Corresponding values of NR and
 346 ISWR at surface decreased monotonically by ~100 W/m² and ~200 W/m², respectively, during
 347 the same period (Figure 2E). Similar to HALT, no daily trend was present in SSA values during
 348 HAHT and SSA values are ~0.9 indicating presence of scattering aerosols (Figure 2B). In
 349 agreement, ADRF values at surface decreased across the week (Figure S1B) with highest values
 350 on high AOD days (14th-15th April; ~150 W/m²) compared to those on low AOD (10th-11th April;
 351 ~50 W/m²). At the same time, the diffuse fraction of incoming radiation at the surface (Figures
 352 S1E) increased substantially from ~0.5 (on 10th April) to ~0.7 on (15th April) during HAHT
 353 indicating strong impact of aerosol loading.

354 In contrast, during LAHT week, the gradient of AOD values from 10th and 15th May, 2017 was
 355 relatively minor (Figure 2C). As the increase in AOD through the week was smaller compared to
 356 other two cases, corresponding decrease of NR and ISWR values at surface was also smaller in
 357 magnitude (~30 W/m²) during this period (Figure 2F). Correspondingly, negligible trend in
 358 ADRF (Figures S1C) at the surface is observed indicating low variation in aerosol radiative
 359 effect change during the LAHT week. Moreover, the midday SSA values during LAHT are
 360 lower (~0.8) compared to HALT and HAHT cases indicating presence of highly absorbing
 361 aerosols in the column (Figure 2C). Accordingly, the ADRF values at surface during LAHT
 362 (Figure S1C) were very high, more than double of the same during HALT and HAHT (i.e. ~350
 363 W/m²). This can be explained by the fact that absorbing aerosols (lower SSA values) were
 364 relatively dominant during LAHT compared to the other 2 cases. Moreover, dominance of
 365 absorbing aerosols also lead to minor variation in diffused radiation during the week (Figure
 366 S1F). To sum up, the impact of aerosol variability (i.e. the gradient in direct radiative effect and
 367 diffused fraction modulation) is minor during the week compared to HAHT and HALT weeks.

369
 370 As aerosol direct radiative effect induces surface cooling, midday T_{srf} values reduced
 371 from ~35°C during low AOD days to ~30°C during high AOD days across the HALT week
 372 (Figure 3A). At the same time, the variability in T_{air} values remain more or less constant during
 373 HALT. Therefore, the midday variation of temperature difference between T_{srf} and T_{air} ($\Delta T = T_{srf}$

Deleted: ,

Deleted: Similarly

Deleted: were also

Deleted: Diffuse_{frac}

Deleted: linearly

Deleted: 6

Deleted: increase in diffuse solar radiation

Deleted: with

Formatted: Font: Not Italic

Formatted: Normal (Web), Indent: First line: 0 cm, Line spacing: 1.5 lines, Adjust space between Latin and Asian text, Adjust space between Asian text and numbers

Formatted: Font: Not Italic

Deleted: In contrast, during LAHT case the variation of AOD values between 11th and 15th May, 17 is relatively minor from ~0.84 to ~1.2, respectively (Figure 2C). As the increase in AOD is smaller compared to other two cases, corresponding decrease of NR and ISWR values at surface is also smaller in magnitude (~30 W/m²) during this period.

Deleted: more

Deleted: Interestingly,

Deleted: However, no significant daily variability in ADRF and Diffuse_{frac} at the surface (Figures S1F) is observed indicating insignificant aerosol radiative effect at daily scale during LAHT (as also seen in Figure 2F).

Formatted: Line spacing: 1.5 lines

Deleted: ADRF

Deleted: in

Deleted: , respectively

Deleted: ,

Deleted: calculated as the difference between

399 T_{air} is inversely proportionally with aerosol loading for HALT (Figure 3A). Greater the value
400 of ΔT , greater will be the turbulent and convection flux, and greater is the tendency of SH flux
401 release at surface. Consequently, sensible heat fluxes are also inversely proportional to increase
402 in AOD (and aerosol direct effect). With increase (decrease) in ΔT (AOD) values, the
403 corresponding SH values increased linearly from $\sim 60 \text{ W/m}^2$ on 2nd June to $\sim 120 \text{ W/m}^2$ on 9th
404 June, 2016 during HALT week (Figure 3D).

405
406 By contrast, a distinct and steep increase in midday T_{air} ($\sim 10 \text{ }^\circ\text{C}$) is seen during HAHT
407 and LAHT weeks. Correspondingly, the mid-day T_{srf} values are also seen to be increasing in
408 close coupling with the T_{air} values during these two weeks (Figures 3B-C). This coupling is
409 mainly because of the coexisting stagnant scenario under heatwave periods. Nonetheless, ΔT
410 variation is inversely proportional to AOD variation during both the weeks (Figure 3B-C).
411 Because, some portion of the enhancement in midday T_{srf} is compensated by the aerosol-induced
412 surface cooling, steeper AOD trend across the week means greater ΔT magnitude. For instance,
413 as aerosol radiative effect is relatively smaller across the week during LAHT compared to that
414 during HAHT, a relatively larger decrease in daily ΔT ($> 2 \text{ }^\circ\text{C}$) is observed during HAHT week
415 (Figure 3B). Consistently, the magnitude of SH also significantly decreased across the week in
416 HAHT and LAHT. Specifically, the midday mean values of SH decreased linearly from ~ 200
417 W/m^2 on 10th April (low AOD) to $\sim 100 \text{ W/m}^2$ on 15th April, 2017 (high AOD) during HAHT
418 (Figure 3E). During LAHT, the midday mean SH decreased linearly from $\sim 200 \text{ W/m}^2$ on 11th
419 May to $\sim 125 \text{ W/m}^2$ on 14-15th May, 2017 (Figure 3F).

420
421 The midday latent heat values decreases by $\sim 150 \text{ Wm}^{-2}$ from high AOD days to low
422 AOD days during HALT week (Figure 3D). In comparison, the increase in LH values with
423 increase in AOD across the HAHT week from 10th April, 2017 to 15th April, 2017 is gradual i.e.
424 $\sim 25 \text{ W/m}^2$ (Figure 3E). Specifically, the slope of regression of latent heat against AOD is 70
425 $\text{W/m}^2/\text{AOD}$ and $10 \text{ W/m}^2/\text{AOD}$ for HALT and HAHT cases, respectively (figure not shown).
426 As, VPD values increase steeply in HAHT case (Figure 3H), but no distinct variation in VPD
427 across the week was evident for HALT case (Figure 3G). Examination of corresponding midday
428 values of gross primary production (GPP) flux (Figures 3G-F) also illustrate gradients similar in
429 sign to corresponding latent heat fluxes indicating that the daily variation in LH flux in both the

Deleted: and

Deleted: SH

Deleted: is

Deleted: ADRF

Deleted: SH

Deleted: till

Deleted: by

Deleted: †

Deleted: †

Deleted: daily

Deleted: cases

Deleted: Further

Deleted: variability

Deleted: is

Deleted: corresponding

Deleted: variability

Deleted: cases

Deleted: daily

Deleted: ADRF

Deleted: during midday

Deleted: ADRF

Deleted: ADRF

Deleted: variation

Deleted: by

Deleted: is observed during HAHT

Deleted: SH

Deleted: mean

Deleted: SH

Deleted: †

Deleted: LH

Deleted: However

Deleted: LH

Deleted: (HAHT case) is much gradual i.e. $\sim 25 \text{ W/m}^2$

Deleted: gradient

Deleted: LH

465 cases is mainly due to associated variation in evapotranspiration. Keeping in mind that the
466 magnitude of AOD variation in both the above cases are similar, the differences in slopes of LH-
467 AOD regression (lower value during HAHT) could be attributed to the simultaneous suppression
468 of evapotranspiration by VPD rise during HAHT week.

470 VPD-associated decline in GPP and thus LH fluxes is even more clearly observed during
471 LAHT week. A strong negative trend in midday values of latent heat and GPP is observed as the
472 week progressed from low to high VPD during LAHT (Figure 3F and 3I). Quantitatively, the
473 slope of regression of (midday mean) latent heat against T_{air} is $+4.1 \text{ W/m}^2/\text{°C}$ and $-6.6 \text{ W/m}^2/\text{°C}$
474 for HAHT and LAHT cases, respectively. Note that the magnitude of VPD variation in both the
475 cases is similar, so the differences in slope of latent heat and T_{air} regression can be attributed to
476 the corresponding differences in aerosol loading. Thus, the magnitude of latent heat or GPP is
477 directly proportional to changes in magnitude of AOD (as seen in HAHT), but the same is
478 inversely proportional to variations in T_{air} or VPD (as seen in LAHT), and the net effects can
479 largely compensate each other (as seen in HAHT).

481 Moreover, the gradient in EF was substantial only in HAHT and HALT where there was
482 substantial variation in AOD across the week. Partitioning of surface energy into latent heat or
483 the latent heat fraction (LHF: Latent heat / Net radiation) decreased and that into sensible heat
484 fraction (SHF: Sensible heat / Net Radiation) increased with increase in AOD across the week
485 during HALT (Figure 3J). As a result, the midday EF distribution decreased with reduction in
486 AOD from ~ 0.8 on 2nd June to ~ 0.6 on 9th June during HALT (Figure 3J). On the same line,
487 with increase in AOD across the week during HAHT, EF also increased from ~ 0.63 on 10th
488 April, 2017 to ~ 0.78 on 15th April, 2017 (Figure 3K) due to simultaneous decrease and increase
489 in SHF and LHF, respectively. But, in absence of clear aerosol gradient across the week, no
490 substantial variation was observed in EF across the week during LAHT case (Figure 3L). The
491 decrease in sensible heat with VPD enhancement was similar in HAHT and LAHT cases (Figure
492 3K-L). But, LH release increased (decreased) with VPD during the former (later) case indicating
493 a role of AOD change on VPD-EF association.

Deleted: is ...re similar, the differences in slopes of LH ...H-
gradient with ...OD regression (lower value during HAHT) could be
induced ...tributed to by AOD...he simultaneous suppression
of VPD...LH nonlinear linkages...vapotranspiration by VPD rise in
during HAHT week. Examination of corresponding midday values of
of GPP (Figures 3G-F) also illustrate daily variations similar in sign
to corresponding LH flux indicating that the daily variation in LH in
both the cases is mainly due to associated variation in
evapotranspiration. (... [1])

Formatted: Indent: First line: 1.27 cm, Line spacing: 1.5
lines

Deleted: LH ...H fluxes is even more clearly observed in ...uring
LAHT case...week. A strong negative trend in midday values of LH
latent heat and GPP is observed as the week progressed from low to
high VPD during LAHT (Figure 3F and 3I). Quantitatively, the
gradient ...lope of regression of (midday mean) LH (... [2])

Deleted: L ... and LAHT cases, respectively. ¶
...Again, n...te that the magnitude of VPD variation in both the
cases is similar, so the differences in slope of LH...latent heat (... [3])

Deleted: inferred to...tributed to be primarily induced by
relatively...he corresponding differences in aerosol loading. Thus,
the changes in ...agnitude of LH (... [4])

Deleted: /...PD (as seen in LAHT), and the relative (... [5])

Formatted: Line spacing: 1.5 lines

Formatted: Indent: First line: 0 cm, Line spacing: 1.5 lines

Moved (insertion) [2]

Deleted: However, no substantial variation was observed in EF
across the week during LAHT case (Figure 3L). ¶
It is interesting to note that variation in EF was only seen in cases
where there was an associated variation in AOD. ...artitioning of
surface energy into LH ...latent heat or the latent heat fraction (LHF:
LHF: ...latent heat H... Net radiation R) ...ein...reased and that into
sensible heat fraction (SHF: SHF (...ensible heat H... Net
Radiation))...inde...reased with increase in AOD during ...cross the
week during HALT (Figure 3J). As a result, the midday EF
distribution decreased with reduction in AOD from ~ 0.8 on 2nd June
to ~ 0.6 on 9th June during HALT (Figure 3J). Similarly...n the same
line, with increase in AOD across the week during HAHT, EF also
increased from ~ 0.63 on 10th April, 2017 to ~ 0.78 on 15th April, 2017
(Figure 3K) during HAHT ...ue to simultaneous decrease and
increase in SHF ...HF and LHF...HF at the same time (... [6])

Moved up [2]: However, no substantial variation was observed in
EF across the week during LAHT case (Figure 3L). The decrease in
SHF sensible heat with VPD enhancement was similar in HAHT and
and LAHT cases (Figure 3K-L). But, LHF LH release increased

Deleted: However, no substantial variation was observed in EF
EF across the week during LAHT case (Figure 3L). ...he decrease in
SHF ...ensible heat with VPD enhancement was similar in HAHT
and LAHT cases (Figure 3K-L). But, LHF ...H release increased
(decreased) with VPD during the former (later) case indicating a role
of AOD change on LH-...PD-EF pathways...ssoication. ¶ (... [7])

659 Figure 4 illustrates the variation in midday mean canopy resistance during the LAHT and
660 HAHT weeks to various physical and physiological factors that control evapotranspiration,
661 namely moisture demand, available energy, air temperature and the aerodynamic resistance. As
662 expected, the canopy resistance is significantly ($p < 0.05$) correlated with VPD although clear
663 differences in the slope is present for the two cases. Specifically, the canopy resistance increases
664 steeply from 400 to 1400 $s\ m^{-1}$ with increase in VPD from 40 to 70 hPa during LAHT case
665 (Figure 4a). However, the canopy resistance only increases from 400 to 500 with an increase in
666 VPD from 45 to 65 hPa during HAHT case (Figure 4a). Similarly, air temperature during these
667 periods also shows a statistically significant positive relationship with canopy resistance (Figure
668 4d). However, during both periods, canopy resistance was found to be independent of available
669 energy (Figure 4c) and the aerodynamic resistance (Figure 4d), indicating that the sensitivity of
670 canopy resistance to changes in VPD (or T_{air}) is significantly greater than that for the other
671 variables.

672 The LAHT case illustrates the frequently reported behaviour of reduction of canopy
673 conductance under increasing VPD due to partial stomata closure as a physiological stress
674 response (Grossiord et al., 2020). Similar responses are also reported in Napier grasses, the
675 native vegetation over our site (Mwendia et al. 2016). Napier grasses can be anisohydric, i.e.
676 water spending under ample water availability (Cardoso et al., 2015). But their behaviour
677 becomes isohydric under high temperature and high water stress (Liang et al., 2017; Mwendia et
678 al. 2014; Purbajanti et al., 2012). During both HAHT and LAHT weeks, soil moisture is very
679 low, hence, the Napier grasses behaves isohydrically under high VPD. The comparison of LAHT
680 and HAHT scatter illustrates that canopy conductance is not strongly affected even under severe
681 VPD rise when aerosol loading also increases in phase. Specifically, the strong gradient of
682 increase in canopy resistance with VPD/ air temperature gets moderated under the high aerosol
683 scenario. Thus, under the presence of high aerosol loading, the isohydric response of Napier
684 grass to temperature rise or the physiological stress under high VPD is decoupled. This can
685 partially explain the aerosol-induced increase in EF (as well as LH and GPP) even under high
686 VPD rise during HAHT.

687 Further, meteorological co-variability or any significant differences in weekly pattern of
688 other micro-meteorological variables between HAHT and LAHT cases can also contribute to the
689 corresponding differences in AOD-VPD-EF association. A closer look illustrates that minor

Formatted: Font: Not Italic

Formatted: Line spacing: 1.5 lines

Formatted: Normal (Web), Line spacing: 1.5 lines

690 gradients are present in the meteorological variables (Figure S2), which can have secondary
691 effects on the VPD-EF associations. Nonetheless, the individual or relative contribution of these
692 meteorological variability and aerosols on the observed coupling remains unknown and deserves
693 further attention in future studies with in depth mechanistic modelling.

694 5. Discussion:

695 The increase in scattering aerosols increased diffused radiation during HALT; thereby
696 facilitating relatively more photosynthesis and thus more GPP and latent heat release with
697 increase in AOD. At the same time, increase in AOD also decreased the temperature difference
698 between surface and air and constrained sensible heat release, eventually leading to aerosol-
699 mediated increase in EF during HALT. However, previous studies investigating the role of
700 aerosols on surface energy fluxes over India have largely reported that aerosol loading is
701 inversely related to latent heat [Murthy et al., 2014; Latha et al., 2019; Gupta et al., 2020].
702 Possible explanations for this apparent contradiction are as follows. First, these studies did not
703 explicitly account for the effect of daily meteorology/ VPD/ temperature variability in their
704 analysis which can have confounding effects (as shown here and discussed in Steiner et al.,
705 2013). Second, these studies were not focused on grassland. Murthy et al., 2014 used
706 micrometeorological site data with a forested footprint in Ranchi. At the same time, Latha et al.,
707 2019 performs analysis at 100 km spatial resolution from reanalysis product/Model, which is
708 representative of a composite land use (including cities, forest, cropland and grassland) and thus
709 a mixture of evapotranspiration and ground evaporation. Gupta et al., 2020 used
710 micrometeorological observations within a typical university canopy (buildings, roads and trees)
711 in Mumbai. Note that total LH can decrease due to aerosols and EF can still increase if SH is
712 decreasing more than EF due to reduction in available energy. Nonetheless, our finding of direct
713 proportionality between aerosol loading and latent heat (or photosynthesis) is consistent with
714 previously reported in-situ studies over grasslands sites in USA [Niyogi et al., 2004; Gu et al.,
715 2002; Wang et al., 2008].

716 In contrast, aerosol loading and heatwave conditions both supressed sensible heat release.
717 Greater aerosol direct radiative effect induces more surface cooling (Chakraborty and Lee,

Deleted: Figure 4 illustrates that the canopy resistance increases steeply from 400 to 1400 s m⁻¹ with increase in VPD from 40 to 70 hPa during LAHT case. However, the canopy resistance increases from 400 to 500 with increase in VPD from 45 to 65 hPa during HAHT case. The LAHT case illustrates the frequently reported behaviour of reduction of canopy conductance under increase in VPD due to partial stomata closure as a physiological stress response. Interestingly, the comparison of LAHT and HAHT scatter illustrates that canopy conductance is not much affected even under severe VPD rise when aerosol loading also increases in phase. This may indicate that under high aerosol loading vegetation gets relatively decoupled from the physiological stress of VPD increase. This can partially explain the aerosol-induced increase in EF (as well as LH and GPP) even under high VPD rise during HAHT. ↴

Moved (insertion) [1]

Formatted: Font colour: Background 2

Deleted: Interestingly, the comparison of LAHT and HAHT scatter illustrates that canopy conductance is not much affected even under severe VPD rise when aerosol loading also increases in phase. This may indicate that under high aerosol loading vegetation gets relatively decoupled from the physiological stress of VPD increase. This can partially explain the aerosol-induced increase in EF (as well as LH and GPP) even under high VPD rise during HAHT. ↴

Moved up [1]: Interestingly, the comparison of LAHT and HAHT scatter illustrates that canopy conductance is not much affected even under severe VPD rise when aerosol loading also increases in phase. This may indicate that under high aerosol loading vegetation gets relatively decoupled from the physiological stress of VPD increase. This can partially explain the aerosol-induced increase in EF (as well as LH and GPP) even under high VPD rise during HAHT. ↴

Formatted: Line spacing: 1.5 lines

Deleted: Diffuse_{fac}

Formatted: Normal (Web), Indent: First line: 0 cm, Line spacing: 1.5 lines

Deleted: LH

Deleted: ΔT

Deleted: SH

Deleted: induced

Deleted: LH

Deleted: or LHF

Formatted: Font: (Default) Times New Roman, 12 pt

Deleted: LH

Deleted: ↴

Formatted: Font colour: Text 1

Formatted: Line spacing: 1.5 lines

Deleted: reduced

Deleted: SH

Deleted: ADRE

Deleted: values

763 2019), and hence lower **sensible heat** fluxes (Yu et al., 2002; Urankar et al., 2012; Steiner et al.,
 764 2013), **as** seen in HALT case. Simultaneously, sensible heat release is also directly proportional
 765 to **the near surface temperature gradient** during Pre-monsoon (Rao et al., 2019), which is **clearly**
 766 **seen** in LAHT case. In HAHT case, both the effects work in phase to **supress, release of sensible**
 767 **heat**. The reduction of **sensible heat** per unit change of T_{air} is $8 \text{ W/m}^2/^{\circ}\text{C}$ during LAHT
 768 compared to the same being $11 \text{ W/m}^2/^{\circ}\text{C}$ in HAHT case. At the same time, the reduction of
 769 **sensible heat** per unit change of AOD is $135 \text{ W/m}^2/\text{AOD}$ during LAHT compared to the same
 770 being $65 \text{ W/m}^2/\text{AOD}$ in HALT case. Hence, increase in AOD and T_{air} , both suppress the release
 771 of available surface energy via **sensible heat** and the effect is largely additive. Moreover, the
 772 intensity of the AOD-induced **sensible heat** suppression will be stronger if the aerosols are
 773 composed of relatively more absorbing aerosols, specifically black carbon [Myhre et al., 2018].
 774 Because, they not only cools the T_{srf} (Mallet et al., 2009; Pandithurai et al., 2008a; Shen et al.,
 775 2020) but also can warm T_{air} (especially under stagnant/heatwave conditions), thereby reducing
 776 **the near surface temperature gradient** and inducing lower tropospheric stability [Dave et al.,
 777 2020; Steiner et al., 2013; Myhre et al., 2018].

778
 779 However, contrary to our results, a recent modelling study over India reports that
 780 enhancement of absorbing aerosols **are positively associated with** increase in **sensible heat and**
 781 **air temperature under heatwave scenario** [Mondal et al., 2020]. The inherent model biases in the
 782 aerosol properties and concentration as well as absence of detailed **canopy-atmosphere** processes
 783 in the model simulations of Mondal et al., 2020 may cause differences in the signature of the
 784 AOD-**sensible heat** feedback. At the same time, the above differences can also be explained by
 785 taking into consideration the difference in time-scale of the feedback used in analysis. For
 786 example, a robust positive association between morning time black carbon concentrations and
 787 mid-day T_{air} is observed by Talukdar et al., 2020. Although, they attributed this association
 788 primarily to diurnal **evolution of the** residual layer mixing, **the understanding from our study can**
 789 also explain a possible pathway. High black carbon loading during morning time can suppress
 790 instantaneous **sensible heat** release (via reduction in the **near surface temperature gradient**),
 791 followed by release of the additional **sensible heat** amount in the mid-day period under relatively
 792 unstable atmosphere (and lower black carbon concentration due to dilution effect). As such,
 793 correlations between absorbing aerosols and **sensible heat** at instantaneous scale can be negative

- Deleted: could
- Deleted: SH
- Deleted: which is also
- Deleted: ΔT
- Deleted: near surface
- Deleted: illustrated
- Deleted: reduce
- Deleted: SH
- Deleted: SH
- Deleted: SH
- Deleted: SH
- Deleted: SH
- Deleted:
- Deleted: ΔT
- Formatted: Indent: First line: 1.27 cm, Line spacing: 1.5 lines
- Deleted: under heatwave scenario causes
- Deleted: SH
- Deleted: along with
- Deleted: aerosol-plant
- Deleted: SH
- Deleted: ity
- Deleted: in
- Deleted: our
- Deleted: here
- Deleted: SH
- Deleted: ΔT
- Deleted: SH
- Deleted: SH

821 (as seen in HAHT), but correlations or composite analysis at daily or monthly time scale may
822 involve feedbacks which can result in positive associations (as also seen in Mondal et al., 2020).

823 In addition, our results clearly underline the complexity and non-linearity between
824 aerosol, VPD and EF, and provides observational evidence to the discussions reported in Steiner
825 et al., 2011; 2013. Keeping all other factors relatively constant, increase in scattering aerosols
826 causes a positive AOD-EF association (as seen in HAHT). In case of HAHT, as both AOD and
827 VPD increased in phase over the week, VPD-induced reduction in evapotranspiration
828 compensated a major portion of the aerosol fertilization effect resulting in a slight increase in
829 latent heat with increase in AOD. Also note that, combined effect of increase in AOD and T_{air}
830 caused a large suppression in sensible heat fluxes. Thus, EF also increases with AOD under
831 heatwave conditions. However, in absence of significant aerosol variation, the increase in VPD
832 causes a large reduction in evapotranspiration (as seen in LAHT). First, negligible aerosol
833 fertilization effect and second, increase in canopy resistance (via stomatal aperture reduction)
834 under steep rise in VPD values caused large reduction in latent heat across the week during
835 LAHT. High VPD is also linked with greater T_{air} during heatwave scenarios, thereby inducing
836 reduction the near surface temperature gradient and sensible heat during LAHT. Thus, both
837 sensible heat and latent heat release decreased with VPD causing negligible change in EF with
838 VPD. Thus, the VPD-EF coupling is very strong in absence of aerosol loading but weakens
839 under aerosol loading. Along with aerosol fertilization effect, the direct deposition of aerosols as
840 a wax layer on the leaf surface can also contribute to such an effect [Burkhardt., 2010; Burkhardt
841 and Grantz., 2017]. Recently, Grantz et al. 2018 used direct observations in glasshouses to
842 illustrate decoupling of stomata conductance (flux-based) from its porosity (higher VPD induces
843 reduction in pore size) under more aerosol scenario. India's mean temperature is constantly
844 rising [Krishnan et al., 2020]. At the same time, the global mean VPD is increasing with global
845 warming [Yuan et al., 2019] and heatwaves will be more frequent in future India [Mukherjee et
846 al., 2018]. Moreover, anthropogenic emissions over Indian Subcontinent will ensure high AOD
847 values in near future [Kumar et al 2018], thus manifesting a HAHT-like scenario at longer time
848 scales over India. Although, the response of plants and crops to enhancement in VPD in warmer
849 future is uncertain, but aerosol-induced weakening of VPD-EF associations can contribute
850 towards tendency of crops and vegetations becoming less drought/heat-resilient in future.

Deleted: ¶

Deleted: suggest

Formatted: Line spacing: 1.5 lines

Deleted: LH

Deleted: Diffuse_{net}-induced increase in LH

Deleted: net

Deleted: LHF

Deleted: decrease

Deleted: SHF

Deleted: LH and LHF

Deleted: ADFE

Deleted: can explain the

Deleted: LHF

Deleted: in ΔT

Deleted: SHF

Deleted: SHF

Deleted: LHF

Deleted: an increase in midday ground heat flux during heatwave events and

Deleted: Moreover, the increase in ground heat flux results in an increase in T_{sf} (as seen in HAHT and LAHT cases) thereby feeding the reduction in ΔT and SHF in the first place.

Deleted: when

Deleted: increases

Deleted: ¶

876
877
878
879
880
881
882
883
884
885
886
887
888
889
890
891
892
893
894
895
896
897
898
899
900
901
902
903
904
905
906

6. Summary

In summary, simultaneous observations from AERONET and an eddy covariance flux tower equipped with micrometeorological and soil physics sensors were employed to report possible influence of aerosol loading on VPD-Evaporative Fraction associations over a natural C4 grassland site under clear sky conditions in the central Gangetic Plains. The main findings from this study are:

1. Increase in aerosol loading reduces the incoming solar radiation at surface and reduces the gradient between surface temperature and near-surface air temperature. This is associated with the decrease in energy dissipation from surface via sensible heat. At the same time, increase in aerosol loading increases the evapotranspiration efficiency of ecosystem by increasing diffuse radiation. Thus, high aerosol loading favors dissipation of available surface energy via Latent heat flux and therefore increases Evaporative fraction.
2. Increase in surface temperature and VPD during heatwave conditions induce larger canopy resistance and stomata closure, thereby reducing the LH fluxes and EF. Native Plants tend to store more water by transpiring less in high temperature conditions; so GPP (and thus LH) reduces under high temperatures. At the same time, higher air temperature, also reduces the sensible heat partitioning via reduction in near surface temperature gradient. Thus, as the effect of VPD involves reducing both the surface fluxes, the net effect on EF is negligible.
3. The variability in aerosol loading tends to play a significant role in modulating the VPD-EF association under varying VPD/surface temperature. When the changes in VPD and scattering aerosols are in phase, like in case of stagnant heat wave conditions over North India, the VPD-induced reduction in evapotranspiration may be completely compensated. This physiological changes can be due to the aerosol fertilization effect or thick aerosol deposition/coating on leaves. Besides, as both increasing AOD and T_{air} induces suppression in sensible heat partitioning, largely the changes in net EF remains in phase with changes in AOD and VPD.

Deleted: ¶

India's mean temperature has already increased by ~ 0.7 degree Celsius since 1900 and is projected to rise by ~4.5 degree Celsius by the end of 2100 relative to present day scenario [Krishnan et al., 2020]. At the same time, the global mean VPD is increasing with global warming [Yuan et al., 2019] and heatwaves will be more frequent in future India [Mukherjee et al., 2018]. Moreover, anthropogenic emissions over Indian Subcontinent will ensure high AOD values in near future [Kumar et al 2018], thus manifesting a HAHT scenario in future India. In this context, our finding that aerosols can reduce the VPD-induced physiological stress on vegetation can have substantial implications. Although, the exact pathway is still not clear, the phenomena of aerosol-induced weakening of the physiological-response by vegetation can make plants and trees less heat-resilient in future. While ADFE can be a potential pathway of aerosol-induced VPD-EF decoupling, possible physiological changes in stomata aperture due to direct deposition of aerosols as a wax layer can also contribute [Burkhardt., 2010; Burkhardt and Grantz., 2017]. Recently, Grantz *et al.* 2018 used direct observations in glasshouses to illustrate similar uncoupling of stomata conductance (flux-based) from its porosity (higher VPD induces reduction in pore size) under more aerosol scenario. Nonetheless, the sensitivity and sign of the AOD-VPD-EF associations depends on the region-specific physiological feedback of vegetation, ambient aerosol optical properties, vegetation structure and VWC. Therefore, land process models should be well-constrained with better quantification of aerosol- T_{air} -VPD-EF continuum for accurately projecting future regional climate, crop yield and adaptation strategies. ¶

Deleted: ¶

Deleted: measurements

Deleted: understand

Deleted: -

Deleted: f

Deleted: and their variability with meteorology

Deleted: SH

Deleted: SH

Deleted: lower

Deleted: ΔT

Deleted: SH and LH

Deleted: s

Deleted: LH

Deleted: by the enhancement in LH via ADFE or

Deleted: due to

Deleted: Moreover

Deleted: reduction

Deleted: SH

Deleted: under such conditions is also

955
956 Nonetheless, a few caveats of this study need to be kept in mind. Our analysis, although driven
957 by fundamental theory of land-atmosphere interactions, is statistical in nature with a relatively
958 small sample size. The cases we analyse here are carefully selected to represent the distinct
959 scenarios as far as realistically possible in this region. Thus, minor influences of meteorological
960 co-variability cannot be totally avoided. As such, the quantitative estimation of various
961 associations may have inherent uncertainties and care should be taken before generalizing.
962 Moreover, as literature on plant physiological responses specific to grass variants found in the
963 Indo-Gangetic Basin region are scarce, this study warrants more species-level studies are
964 necessary to isolate the physiological and environmental responses on EF. Nevertheless, the
965 possible AOD-VPD-EF associations discussed here can have substantial implications on future
966 climate of this and similar subtropical regions. Thus, the observational associations provided in
967 this study not only encourages more measurements, detailed in situ experiments and mechanistic
968 modelling of aerosol-vegetation-atmosphere interactions, but also warrants proper
969 representations of aerosol processes and feedbacks in coupled models over India.

Formatted: Font: (Default) Times New Roman, 12 pt, Not Italic,

Deleted: evidence

Formatted: Font: (Default) Times New Roman, 12 pt,

Deleted: ¶
To sum up

Deleted: experiments

Deleted: plant

Deleted: physical and physiological properties

Deleted: land process

Deleted: this region of strong aerosol-land-atmosphere coupling

971 **Acknowledgement:**

972 SNT gratefully acknowledge the financial support given by the Earth System Science
973 Organization, Ministry of Earth Sciences, Government of India (grant MM/NERC-MoES-
974 03/2014/002) and Newton Fund to conduct this research under Monsoon Mission. CS
975 acknowledges support from MHRD, India under project number SB20210835CEMHRD00850.
976 LMM acknowledges the support of the Natural Environment Research Council (NERC) South
977 American Biomass Burning Analysis (SAMBBA) project grant code NE/J010057/1. The authors
978 would like to thank Dr E. J. Welton, B.N. Holben and staff at NASA GSFC for establishing and
979 quality control of the AERONET and MPLNET site at IIT Kanpur, used in this study.

Deleted: ¶

981 **Data statement:**

982 Surface data used here is available at: [https://catalogue.ceh.ac.uk/documents/78c64025-1f8d-](https://catalogue.ceh.ac.uk/documents/78c64025-1f8d-431c-bdeb-e69a5877d2ed)
983 [431c-bdeb-e69a5877d2ed](https://catalogue.ceh.ac.uk/documents/78c64025-1f8d-431c-bdeb-e69a5877d2ed). Aerosol data used here is available from
984 <https://www.iitk.ac.in/ce/aeronet>.

Formatted: Font colour: Text 1

Deleted: ¶

996
997
998
999

References

1. Bollasina, M. A., and Y. Ming (2013), The role of land-surface processes in modulating the Indian monsoon annual cycle, *Climate Dynamics*, 41(9-10), 2497-2509.
2. Campbell, J. R., D. L. Hlavka, E. J. Welton, C. J. Flynn, D. D. Turner, J. D. Spinhirne, V. S. S. III, and I. H. Hwang (2002), Full-Time, Eye-Safe Cloud and Aerosol Lidar Observation at Atmospheric Radiation Measurement Program Sites: Instruments and Data Processing, *Journal of Atmospheric and Oceanic Technology*, 19(4), 431-442.
3. Chakraborty, S., U. Saha, and A. Maitra (2015), Relationship of convective precipitation with atmospheric heat flux — A regression approach over an Indian tropical location, *Atmospheric Research*, 161-162, 116-124.
4. Chameides, W. L., et al. (1999), Case study of the effects of atmospheric aerosols and regional haze on agriculture: An opportunity to enhance crop yields in China through emission controls?, *Proceedings of the National Academy of Sciences*, 96(24), 13626-13633.
5. Collatz, G. J., J. T. Ball, C. Grivet, and J. A. Berry (1991), Physiological and environmental regulation of stomatal conductance, photosynthesis and transpiration: a model that includes a laminar boundary layer, *Agricultural and Forest Meteorology*, 54(2), 107-136.
6. Dey, S., and L. Di Girolamo (2011), A decade of change in aerosol properties over the Indian subcontinent, *Geophysical Research Letters*, 38(14), n/a-n/a.
7. Dimitris, G. K., P. S. Ramesh, G. Ritesh, S. Manish, P. G. Kosmopoulos, and S. N. Tripathi (2012), Variability and trends of aerosol properties over Kanpur, northern India using AERONET data (2001-10), *Environmental Research Letters*, 7(2), 024003.
8. Forster, P., V. Ramaswamy, P. Artaxo, T. Berntsen, R. Betts, D. W. Fahey, J. Haywood, J. Lean, D. C. Lowe, and G. Myhre (2007), Changes in atmospheric constituents and in radiative forcing. Chapter 2, in *Climate Change 2007. The Physical Science Basis*, edited.
9. Gautam, R., N. C. Hsu, and K. M. Lau (2010), Premonsoon aerosol characterization and radiative effects over the Indo-Gangetic Plains: Implications for regional climate warming, *Journal of Geophysical Research: Atmospheres*, 115(D17), n/a-n/a.
10. Gautam, R., et al. (2011), Accumulation of aerosols over the Indo-Gangetic plains and southern slopes of the Himalayas: distribution, properties and radiative effects during the 2009 pre-monsoon season, *Atmos. Chem. Phys.*, 11(24), 12841-12863.
11. Gu, L., T. Meyers, S. G. Pallardy, P. J. Hanson, B. Yang, M. Heuer, K. P. Hosman, J. S. Riggs, D. Sluss, and S. D. Wullschleger (2006), Direct and indirect effects of atmospheric conditions and soil moisture on surface energy partitioning revealed by a prolonged drought at a temperate forest site, *Journal of Geophysical Research: Atmospheres*, 111(D16), n/a-n/a.
12. Jones, H. G., and R. A. Sutherland (1991), Stomatal control of xylem embolism, *Plant, Cell & Environment*, 14(6), 607-612.
13. Liu, S., M. Chen, and Q. Zhuang (2014), Aerosol effects on global land surface energy fluxes during 2003-2010, *Geophysical Research Letters*, 41(22), 7875-7881.

Formatted: Line spacing: 1.5 lines

Deleted: ¶

Field Code Changed

- 1041 14. Mallet, M., P. Tulet, D. Serça, F. Solmon, O. Dubovik, J. Pelon, V. Pont, and O. Thouron
1042 (2009), Impact of dust aerosols on the radiative budget, surface heat fluxes, heating rate
1043 profiles and convective activity over West Africa during March 2006, *Atmos. Chem.*
1044 *Phys.*, 9(18), 7143-7160.
- 1045 15. Matsui, T., A. Beltrán-Przekurat, D. Niyogi, R. A. Pielke, and M. Coughenour (2008),
1046 Aerosol light scattering effect on terrestrial plant productivity and energy fluxes over the
1047 eastern United States, *Journal of Geophysical Research: Atmospheres*, 113(D14), n/a-n/a.
- 1048 16. Murthy, B. S., R. Latha, K. Manoj, and N. C. Mahanti (2014), Effect of aerosols on
1049 evapo-transpiration, *Atmospheric Environment*, 89, 109-118.
- 1050 17. Niyogi, D., H.-I. Chang, F. Chen, L. Gu, A. Kumar, S. Menon, and R. A. Pielke (2007),
1051 Potential impacts of aerosol–land–atmosphere interactions on the Indian monsoonal
1052 rainfall characteristics, *Natural Hazards*, 42(2), 345-359.
- 1053 18. Niyogi, D., et al. (2004), Direct observations of the effects of aerosol loading on net
1054 ecosystem CO₂ exchanges over different landscapes, *Geophysical Research Letters*,
1055 31(20), n/a-n/a.
- 1056 19. Pandithurai, G., C. Seethala, B. S. Murthy, and P. C. S. Devara (2008a), Investigation of
1057 atmospheric boundary layer characteristics for different aerosol absorptions: Case studies
1058 using CAPS model, *Atmospheric Environment*, 42(19), 4755-4768.
- 1059 20. Pandithurai, G., S. Dipu, K. K. Dani, S. Tiwari, D. S. Bisht, P. C. S. Devara, and R. T.
1060 Pinker (2008b), Aerosol radiative forcing during dust events over New Delhi, India,
1061 *Journal of Geophysical Research: Atmospheres*, 113(D13), n/a-n/a.
- 1062 21. Saha, S. K., S. Halder, K. K. Kumar, and B. N. Goswami (2011), Pre-onset land surface
1063 processes and ‘internal’ interannual variabilities of the Indian summer monsoon, *Climate*
1064 *Dynamics*, 36(11), 2077-2089.
- 1065 22. Sarangi, C., S. N. Tripathi, A. K. Mishra, A. Goel, and E. J. Welton (2016), Elevated
1066 aerosol layers and their radiative impact over Kanpur during monsoon onset period,
1067 *Journal of Geophysical Research: Atmospheres*, 121(13), 7936-7957.
- 1068 23. Schwartz, S. E. (1996), Atmospheric AerosolsThe whitehouse effect—Shortwave
1069 radiative forcing of climate by anthropogenic aerosols: an overview, *Journal of Aerosol*
1070 *Science*, 27(3), 359-382.
- 1071 24. Srivastava, A., S. Tiwari, P. Devara, D. Bisht, M. K. Srivastava, S. Tripathi, P. Goloub,
1072 and B. Holben (2011), Pre-monsoon aerosol characteristics over the Indo-Gangetic Basin:
1073 implications to climatic impact, paper presented at *Annales Geophysicae*, European
1074 Geosciences Union.
- 1075 25. Steiner, A. L., and W. L. Chameides (2011), Aerosol-induced thermal effects increase
1076 modelled terrestrial photosynthesis and transpiration, *Tellus B*, 57(5).
- 1077 26. Steiner, A. L., D. Mermelstein, S. J. Cheng, T. E. Twine, and A. Oliphant (2013),
1078 Observed Impact of Atmospheric Aerosols on the Surface Energy Budget, *Earth*
1079 *Interactions*, 17(14), 1-22.
- 1080 27. Trenberth, K. E., J. T. Fasullo, and J. Kiehl (2009), Earth's Global Energy Budget,
1081 *Bulletin of the American Meteorological Society*, 90(3), 311-323.
- 1082 28. Urankar, G., T. V. Prabha, G. Pandithurai, P. Pallavi, D. Achuthavarier, and B. N.
1083 Goswami (2012), Aerosol and cloud feedbacks on surface energy balance over selected
1084 regions of the Indian subcontinent, *Journal of Geophysical Research: Atmospheres*,
1085 117(D4), n/a-n/a.

- 1086 29. Wang, K., and R. E. Dickinson (2012), A review of global terrestrial evapotranspiration:
 1087 Observation, modeling, climatology, and climatic variability, *Reviews of Geophysics*,
 1088 50(2), n/a-n/a.
- 1089 30. Wang, K., R. E. Dickinson, and S. Liang (2008), Observational evidence on the effects of
 1090 clouds and aerosols on net ecosystem exchange and evapotranspiration, *Geophysical*
 1091 *Research Letters*, 35(10), n/a-n/a.
- 1092 31. Welton, E. J., and J. R. Campbell (2002), Micropulse Lidar Signals: Uncertainty Analysis,
 1093 *Journal of Atmospheric and Oceanic Technology*, 19(12), 2089-2094.
- 1094 32. Yu, H., S. C. Liu, and R. E. Dickinson (2002), Radiative effects of aerosols on the
 1095 evolution of the atmospheric boundary layer, *Journal of Geophysical Research:*
 1096 *Atmospheres*, 107(D12), AAC 3-1-AAC 3-14.
- 1097 33. Koster, R. D., Dirmeyer, P. A., Guo, Z., Bonan, G., Chan, E., Cox, P., ... & Liu, P. (2004).
 1098 Regions of strong coupling between soil moisture and precipitation. *Science*, 305(5687),
 1099 1138-1140.
- 1100 34. Turner, A. G., Bhat, G. S., Martin, G. M., Parker, D. J., Taylor, C. M., Mitra, A. K., ... &
 1101 Morrison, R. (2019). Interaction of convective organization with monsoon precipitation,
 1102 atmosphere, surface and sea: The 2016 INCOMPASS field campaign in India. *Quarterly*
 1103 *Journal of the Royal Meteorological Society*.
- 1104 35. Chakraborty, T., & Lee, X. (2019). Land cover regulates the spatial variability of
 1105 temperature response to the direct radiative effect of aerosols. *Geophysical Research*
 1106 *Letters*, 46(15), 8995-9003.
- 1107 36. Chakraborty, T., Sarangi, C., Krishnan, M., Tripathi, S. N., Morrison, R., & Evans, J.
 1108 (2019). Biases in model-simulated surface energy fluxes during the Indian monsoon onset
 1109 period. *Boundary-Layer Meteorology*, 170(2), 323-348.
- 1110 37. Chakraborty, T. C., Lee, X., & Lawrence, D. M. (2021). Strong local evaporative cooling
 1111 over land due to atmospheric aerosols. *Journal of Advances in Modeling Earth Systems*,
 1112 13(5), e2021MS002491.
- 1113
- 1114 38. Rigden, A. J., & Salvucci, G. D. (2017). Stomatal response to humidity and CO₂
 1115 implicated in recent decline in US evaporation. *Global Change Biology*, 23(3), 1140-
 1116 1151.
- 1117 39. Yuan, W., Zheng, Y., Piao, S., Ciais, P., Lombardozzi, D., Wang, Y., ... & Jain, A. K.
 1118 (2019). Increased atmospheric vapor pressure deficit reduces global vegetation
 1119 growth. *Science advances*, 5(8), eaax1396.
- 1120 40. Wang Z., C. Wang, B. Wang, X. Wang, J. Li, J. Wu, L. Liu Interactive effects of air
 1121 pollutants and atmospheric moisture stress on aspen growth and photosynthesis along an
 1122 urban-rural gradient. *Environ. Pollut.*, 260 (2020),
 1123 Article 114076, [10.1016/j.envpol.2020.114076](https://doi.org/10.1016/j.envpol.2020.114076)
- 1124 41. Burkhardt J, Grantz DA. 2017. Plants and atmospheric aerosols. *Progress Botany* 78: 369–
 1125 406
- 1126 42. Burkhardt J. 2010. Hygroscopic particles on leaves: nutrients or desiccants? *Ecological*
 1127 *Monographs* 80: 369–399.
- 1128 43. Grantz DA, Zinsmeister D, Burkhardt J. 2018. Ambient aerosol increases minimum leaf
 1129 conductance and alters the aperture–flux relationship as stomata respond to vapor pressure
 1130 deficit (VPD). *New Phytologist* 219: 275–286.

Formatted: Do not check spelling or grammar, Pattern: Clear

Formatted: Font: (Default) Times New Roman, 12 pt, Font colour: Text 1

- 1131 44. R. Latha, B. S. Murthy & B. Vinayak (2019) Aerosol-induced perturbation of surface
1132 fluxes over different landscapes in a tropical region, *International Journal of Remote*
1133 *Sensing*, 40:21, 8203-8221, DOI: [10.1080/01431161.2018.1523586](https://doi.org/10.1080/01431161.2018.1523586)
- 1134 45. Krishnan et al (2020) Assessment of climate change over the Indian region: a report of the
1135 Ministry of Earth Sciences (MoES), Government of India
- 1136 46. Wang X., J. Wu, M. Chen, X. Xu, Z. Wang, B. Wang, C. Wang, S. Piao, W. Lin, G. Miao,
1137 Deng, C. Qiao, J. Wang, S. Xu, L. Liu, Field evidences for the positive effects of aerosols
1138 on tree growth. *Global Change Biol.*, 24 (2018), pp. 4983-4992
- 1139 47. Myhre, G., Samset, B.H., Hodnebrog, Ø. et al. Sensible heat has significantly affected the
1140 global hydrological cycle over the historical period. *Nat Commun* 9, 1922 (2018).
1141 <https://doi.org/10.1038/s41467-018-04307-4>
- 1142 48. Rao, K. G., & Reddy, N. N. (2019). On moisture flux of the Indian summer monsoon: A
1143 new perspective. *Geophysical Research*
1144 *Letters*, 46, 1794–1804. <https://doi.org/10.1029/2018GL080392>
- 1145 49. Mondal, A, Sah, N, Sharma, A, Venkataraman, C, Patil, N. Absorbing aerosols and
1146 high-temperature extremes in India: A general circulation modelling study. *Int J*
1147 *Climatology*. 2020; 1–20. <https://doi.org/10.1002/joc.6783>
- 1148 50. Shen Z, Ming Y, Held IM. Using the fast impact of anthropogenic aerosols on regional
1149 land temperature to constrain aerosol forcing. *Sci Adv*. 2020 Aug 5;6(32): doi:
1150 10.1126/sciadv.5297.
- 1151 51. Dave P, Bhushan, M., Venkatraman, C., Absorbing aerosol influence on temperature
1152 maxima: An observation-based study over India. *Atmospheric Environment*, Volume 223,
1153 2020, 117237, ISSN 1352-2310, <https://doi.org/10.1016/j.atmosenv.2019.117237>.
- 1154 52. Talukdar S. and M.V. Ratnam, A mutual response between surface temperature and black
1155 carbon mass concentration during the daytime, *Science of the Total Environment*,
1156 <https://doi.org/10.1016/j.scitotenv.2020.143477>
- 1157 53. Knohl, A., and D. D. Baldocchi (2008), Effects of diffuse radiation on canopy gas
1158 exchange processes in a forestecosystem, *J. Geophys. Res.*, 113, G02023,
1159 doi:10.1029/2007JG000663
- 1160 54. Davin, E. L. and Seneviratne, S. I.: Role of land surface processes and diffuse/direct
1161 radiation partitioning in simulating the European climate, *Biogeosciences*, 9, 1695–1707,
1162 <https://doi.org/10.5194/bg-9-1695-2012>, 2012
- 1163 55. O’Sullivan, M., A. Rap, C. L. Reddington, D. V. Spracklen, M. Gloor, and W. Buermann
1164 (2016), Small global effect on terrestrial net primary production due to increased fossil fuel
1165 aerosol emissions from East Asia since the turn of the century, *Geophys. Res. Lett.*,
1166 43, 8060–8067, doi:10.1002/2016GL068965.
- 1167 56. Yue, X. and Unger, N.: Aerosol optical depth thresholds as a tool to assess diffuse
1168 radiation fertilization of the land carbon uptake in China, *Atmos. Chem. Phys.*, 17, 1329–
1169 1342, <https://doi.org/10.5194/acp-17-1329-2017>, 2017.
- 1170 57. Mercado LM, Bellouin N, Sitch S, Boucher O, Huntingford C, Wild M, Cox PM. Impact
1171 of changes in diffuse radiation on the global land carbon sink. *Nature*. 2009 Apr
1172 23;458(7241):1014-7. doi: 10.1038/nature07949. PMID: 19396143.
- 1173 58. Kumar, R., Barth, M. C., Pfister, G. G., Delle Monache, L., Lamarque, J. F., Archer-
1174 Nicholls, S., Walters, S. (2018). How will air quality change in South Asia by
1175 2050? *Journal of Geophysical Research:*
1176 *Atmospheres*, 123, 1840–1864. <https://doi.org/10.1002/2017JD027357>

Formatted: Font: (Default) Times New Roman, 12 pt, Font colour: Text 1

Formatted: Font: (Default) Times New Roman, 12 pt, Font colour: Text 1

Formatted: Font: (Default) Times New Roman, 12 pt, Font colour: Text 1

Formatted: Font: (Default) Times New Roman, 12 pt, Font colour: Text 1

Formatted: Font: (Default) Times New Roman, 12 pt, Font colour: Text 1

1177 59. M. Kumar, K.S. Parmar, D.B. Kumar, A.Mhawish, D.M. Broday, R.K. Mall, T. Banerjee
1178 Long-term aerosol climatology over Indo-Gangetic Plain: trend, prediction and potential
1179 source field; *Atmos. Environ.*, 180 (2018), pp. 37-50

1180 60. Bhat G. S., R. Morrison, C. M. Taylor, B. K. Bhattacharya, S. Paler, D. Desai, J. G.
1181 Evans, S. Pattnaik, M. Sekhar, R. Nigam, A. Sattar, S. S. Angadi, D. Kacha, A. Patidar, S.
1182 N. Tripathi, K. V. M. Krishnan, A. Sisodiya; Spatial and temporal variability in energy
1183 and water vapour fluxes observed at seven sites on the Indian subcontinent during 2017. *Q*
1184 *J R Meteorol Soc.* 2020; 146: 2853–2866. <https://doi.org/10.1002/qj.3688>

1185 61. Ratnam, J., Behera, S., Ratna, S. *et al.* Anatomy of Indian heatwaves. *Sci Rep* 6, 24395
1186 (2016). <https://doi.org/10.1038/srep24395>.

1187 62. Mukherjee, S., Mishra, V. A sixfold rise in concurrent day and night-time heatwaves in
1188 India under 2 °C warming. *Sci Rep* 8, 16922 (2018). [https://doi.org/10.1038/s41598-018-](https://doi.org/10.1038/s41598-018-35348-w)
1189 [35348-w](https://doi.org/10.1038/s41598-018-35348-w)

1190 63. Morrison, R.; Angadi, S.S.; Cooper, H.M.; Evans, J.G.; Rees, G.; Sekhar, M.; Taylor, C.;
1191 Tripathi, S.N.; Turner, A.G. (2019). Energy and carbon dioxide fluxes, meteorology and
1192 soil physics observed at INCOMPASS land surface stations in India, 2016 to 2017. NERC
1193 Environmental Information Data Centre. [https://doi.org/10.5285/78c64025-1f8d-431c-](https://doi.org/10.5285/78c64025-1f8d-431c-bdeb-e69a5877d2ed)
1194 [bdeb-e69a5877d2ed](https://doi.org/10.5285/78c64025-1f8d-431c-bdeb-e69a5877d2ed)

1195 64. Mayank Gupta et al 2021 *Environ. Res. Lett.* 16 014021

1196 65. Rohini, P., Rajeevan, M. & Srivastava, A. On the Variability and Increasing Trends of
1197 Heat Waves over India. *Sci Rep* 6, 26153 (2016). <https://doi.org/10.1038/srep26153>

1198 66. Mwendia, S. W., Yunusa, I. A., Sindel, B. M., Whalley, R. D., & Kariuki, I. W. (2017).
1199 Assessment of Napier grass accessions in lowland and highland tropical environments of
1200 East Africa: water stress indices, water use and water use efficiency. *Journal of the*
1201 *Science of Food and Agriculture*, 97(6), 1953-1961.

1202 67. van Heerwaarden, C. C., & Teuling, A. J. (2014). Disentangling the response of forest and
1203 grassland energy exchange to heatwaves under idealized land-atmosphere
1204 coupling. *Biogeosciences*, 11(21), 6159-6171.

1205 68. Juan Andrés Cardoso, Marcela Pineda, Juan de la Cruz Jiménez, Manuel Fernando
1206 Vergara, Idupulapati M. Rao, Contrasting strategies to cope with drought conditions by
1207 two tropical forage C₄grasses, *AoB PLANTS*, Volume 7, 2015,
1208 plv107. <https://doi.org/10.1093/aobpla/plv107>

1209 69. Liang, X., Erickson, J.E., Sollenberger, L.E., Rowland, D.L., Silveira, M.L. and
1210 Vermerris, W. (2018), Growth and Transpiration Responses of Elephantgrass and
1211 Energycane to Soil Drying. *Crop Science*, 58: 354-
1212 363. <https://doi.org/10.2135/cropsci2017.01.0019>

1213 70. Purbajanti, E.; Anwar, S.; Wydiati, F.K. Drought stress effect on morphology characters,
1214 water use efficiency, growth and yield of guinea and napier grasses. *Int. Res. J. Plant*
1215 *Sci.* 2012, 3, 47. [Google Scholar]

1216 71. Mwendia, S.; Yunusa, I.; Whalley, R.; Sindel, B.; Kenney, D.; Kariuki, I. Use of plant water
1217 relations to assess forage quality and growth for two cultivars of Napier grass (*Pennisetum*
1218 *purpureum*) subjected to different levels of soil water supply and temperature regimes. *Crop*
1219 *Pasture Sci.* 2014, 64, 1008–1019. [Google Scholar]

1220 72. Holm L, Pancho JV, Herberger JP, Plucknett DL, 1979. A Geographical Atlas of World
1221 Weeds. Toronto, Canada: John Wiley and Sons Inc

Formatted: Font: (Default) Times New Roman, 12 pt, Font colour: Text 1

Formatted: Font: (Default) Times New Roman, 12 pt, Font colour: Text 1

Formatted: Font: (Default) Times New Roman, 12 pt, Font colour: Text 1

Formatted: Font: (Default) Times New Roman, 12 pt, Font colour: Text 1

Formatted: Font colour: Text 1

Formatted: Line spacing: single

Formatted: Hyperlink, Font: (Default) +Body (Calibri), 11 pt, Font colour: Auto, Pattern: Clear

Formatted: Pattern: Clear

Field Code Changed

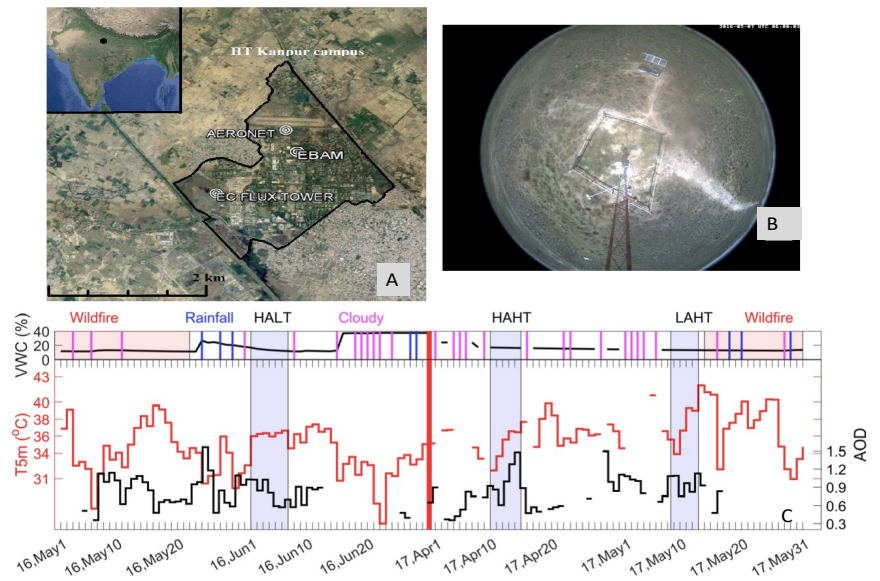
Field Code Changed

Field Code Changed

Field Code Changed

Formatted: Font colour: Text 1

1222 [73. Charlotte Grossiord, Thomas N. Buckley, Lucas A. Cernusak, Kimberly A.](#)
 1223 [Novick, Benjamin Poulter, Rolf T. W. Siegwolf, John S. Sperry, Nate G. McDowell](#)
 1224 [74. Irmak, S., and Mutiibwa, D. \(2010\). On the dynamics of canopy resistance: Generalized](#)
 1225 [linear estimation and relationships with primary micrometeorological variables.](#) *Water*
 1226 [Resour. Res.](#), 46, W08526, doi:10.1029/2009WR008484.



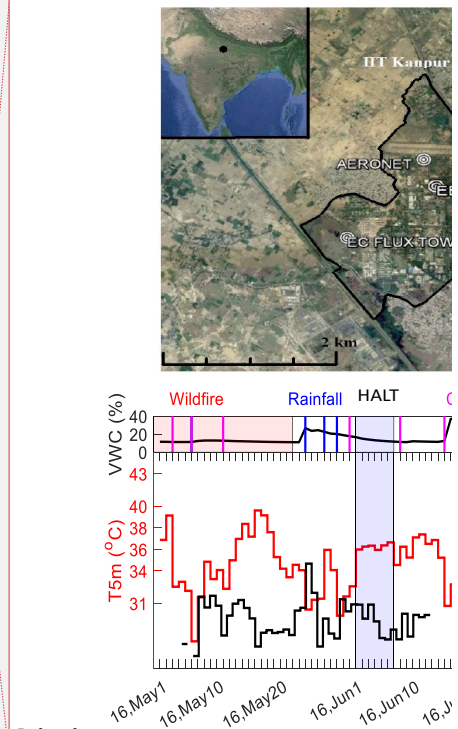
1230
 1231 *Figure 1: A) Map showing the locations of AERONET and the EC flux tower site within the*
 1232 *campus of the Indian Institute of Technology Kanpur (IITK). Inset map shows the location of*
 1233 *IITK (black dot) in the central Gangetic Plains. The maps are created by © Google Maps 2017.*
 1234 *B) Camera image of land cover of the flux tower site during May 12th, 2017. C) Daily variation*
 1235 *in soil moisture (VWC, volumetric water content) during our study period is shown in black line*
 1236 *in upper box of the figure. The occurrences of cloudy days, rainy days and wildfire affected*
 1237 *period during April through June of 2016 and 2017 is shown by magenta, blue and pink colour*
 1238 *patches in the upper box. A cloudy day is inferred from MPLNET images and AERONET*
 1239 *observations (as defined in Section 2 of main text). The days bounded by straight lines depict the*
 1240 *weekly episodes HALT, HAHT and LAHT, respectively. Daily variation in T_{air} and daily*
 1241 *variation in AOD during our study period is shown as black and red lines in lower box of the*
 1242 *panel.*

Formatted: Font: (Default) Times New Roman, 12 pt, Font colour: Text 1

Formatted: Pattern: Clear

Formatted: Indent: Left: 1.13 cm, No bullets or numbering

Deleted: ¶



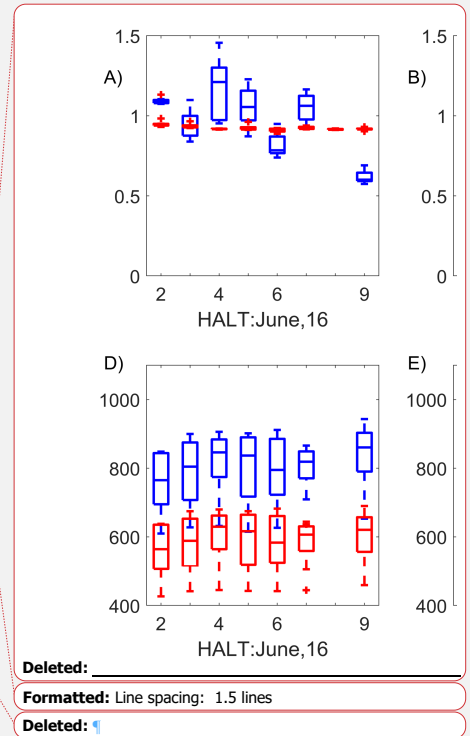
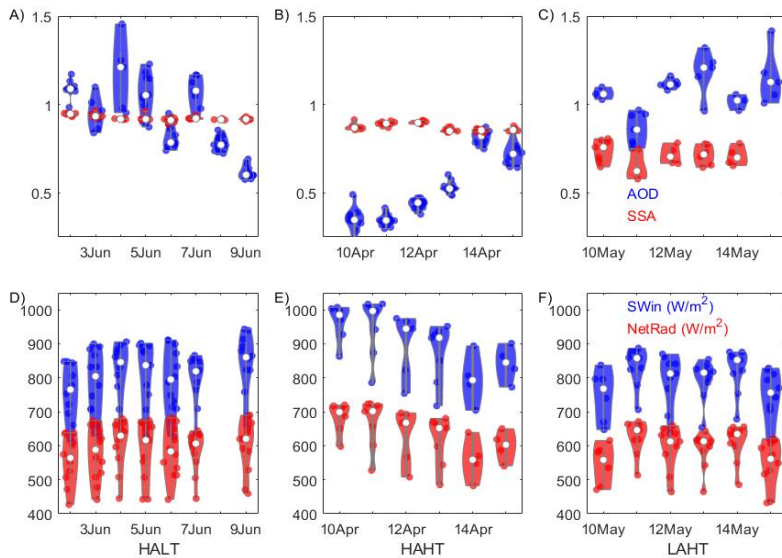
Deleted:

Formatted: Line spacing: 1.5 lines

Formatted: Normal, Indent: Left: 0 cm

Formatted: Font colour: Text 1

Deleted: Daily variation in VWC during our study period is shown in black line in upper box of the figure. The occurrences of cloudy days, rainy days and wildfire affected period during April through June of 2016 and 2017 is shown by magenta, blue and pink colour patches in the upper box. A cloudy day is inferred from MPLNET images and AERONET observations (as defined in Section 2 of main text). The days bounded by straight lines depict the study episodes HALT, HAHT and LAHT, respectively. Daily variation in T_{air} and daily variation in AOD during our study period is shown as black and red lines in lower box of the panel. ¶

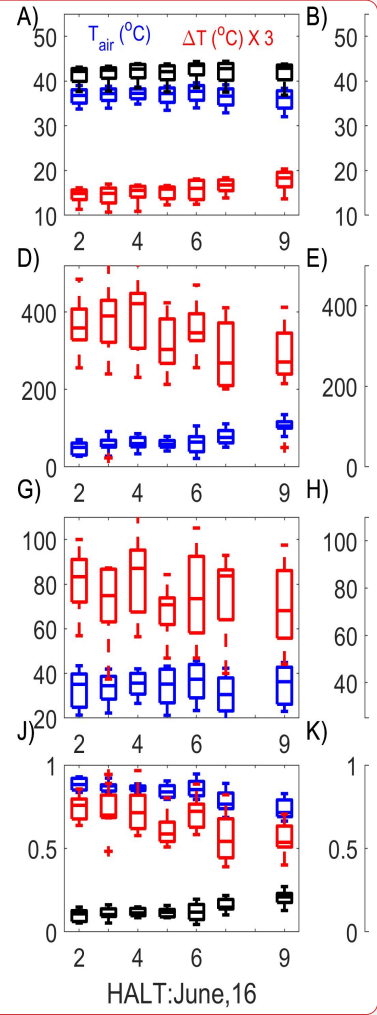
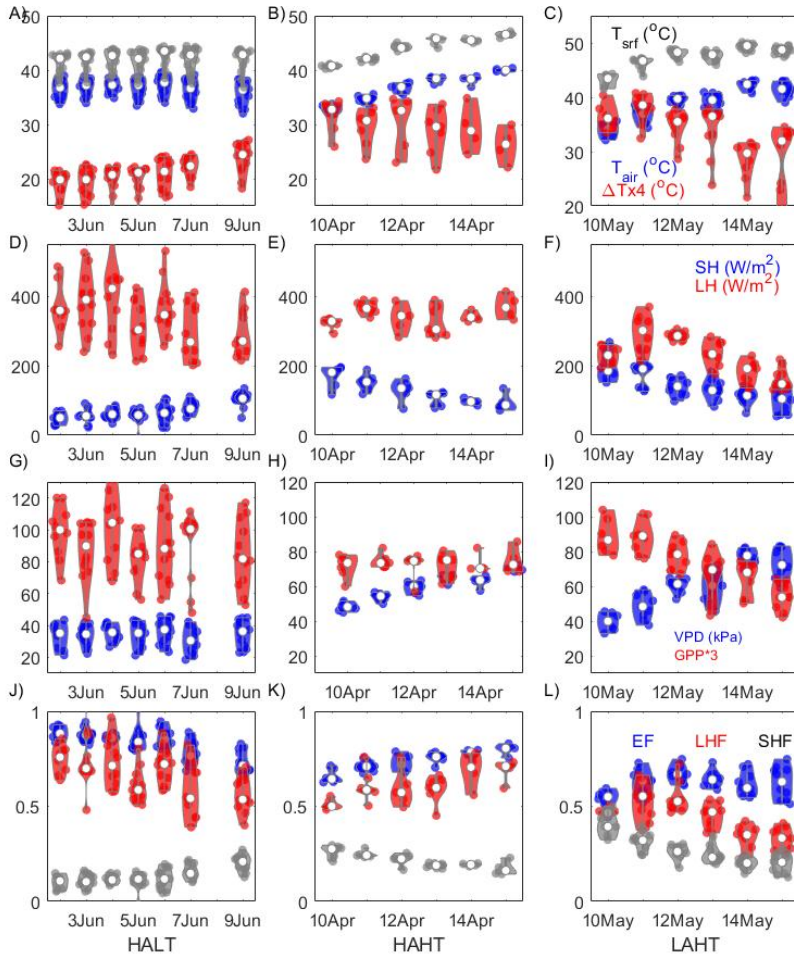


1256

1257 *Figure 2: Distribution plots showing the variations in aerosol and radiation during the cases.*
 1258 *Row 1 illustrates Time series of midday (1100-1400 LT) variation in AOD and SSA values*
 1259 *during HALT, HAHT and LAHT, respectively.. The horizontal line within box represents median*
 1260 *of the distribution. The bottom and top edge of the boxes represent 25th and 75th percentile,*
 1261 *respectively, of the distribution. The short dash at top and bottom extent of the boxes represent*
 1262 *5th and 95th percentile, respectively. Row 2 is same as Row 1 but show measurements of*
 1263 *incoming short wave radiation and net radiation at surface. Note that June,16 means June of*
 1264 *2016 and so on.*

1265

Deleted: Figure 2: Box plots showing the variations in aerosol and radiation during the cases. Row 1 illustrates Time series of midday (1100-1400 LT) variation in AOD and SSA values during HALT, HAHT and LAHT, respectively.. The horizontal line within box represents median of the distribution. The bottom and top edge of the boxes represent 25th and 75th percentile, respectively, of the distribution. The short dash at top and bottom extent of the boxes represent 5th and 95th percentile, respectively. Row 2 is same as Row 1 but show measurements of incoming short wave radiation and net radiation at surface. Note that June,16 means June of 2016 and so on.



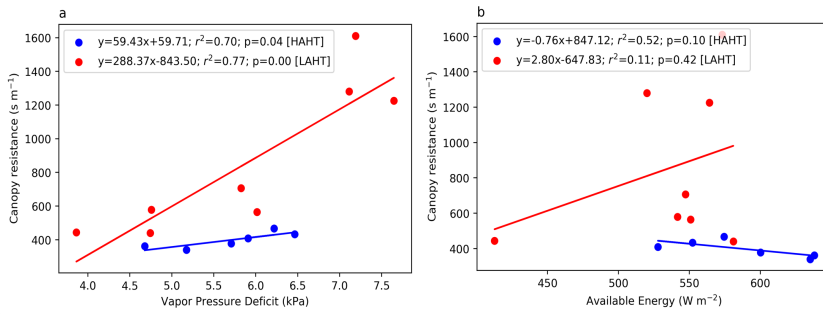
Deleted:
Deleted: ¶

Deleted: Figure 3: Box plots showing the variations in near surface meteorology and surface fluxes during the cases. Row 1 illustrates Time series of midday (1100-1400 LT) variation in T_{srf} , T_{air} and $(-\Delta T)$ values during HALT, HAHT and LAHT, respectively. Row 2 is same as Row 1 but for SH and LH. Row 3 is same but for VPD and GPP ; Row 4 is same but for EF, LHF (red) and SHF. ¶

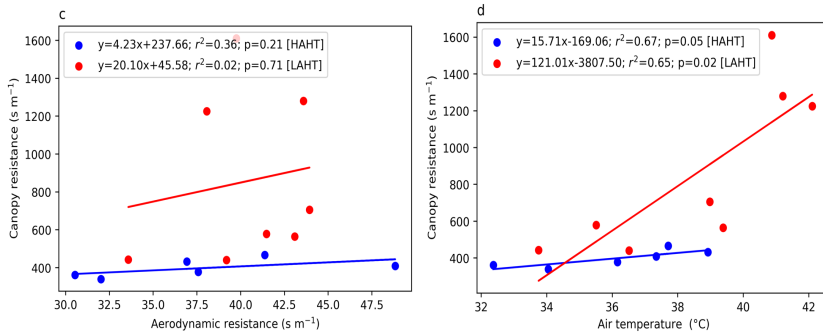
1279
1280
1281
1282
1283
1284
1285

Figure 3: Distribution plots showing the variations in near surface meteorology and surface fluxes during the cases. Row 1 illustrates Time series of midday (1100-1400 LT) variation in T_{srf} , T_{air} and $(-\Delta T)$ values during HALT, HAHT and LAHT, respectively. Row 2 is same as Row 1 but for SH and LH. Row 3 is same but for VPD and GPP ; Row 4 is same but for EF, LHF (red) and SHF.

1294



1295



1296

1297

1298

1299

Figure 4: Linear correlation between daily midday average Canopy resistance derived from Penman-Monteith equation *with a) observed Vapor Pressure Deficit (VPD); b) Available energy at surface; c) Aerodynamic resistance and d) Air temperature* for HAHT and LAHT cases.

1300

1301

1302

1303

1304

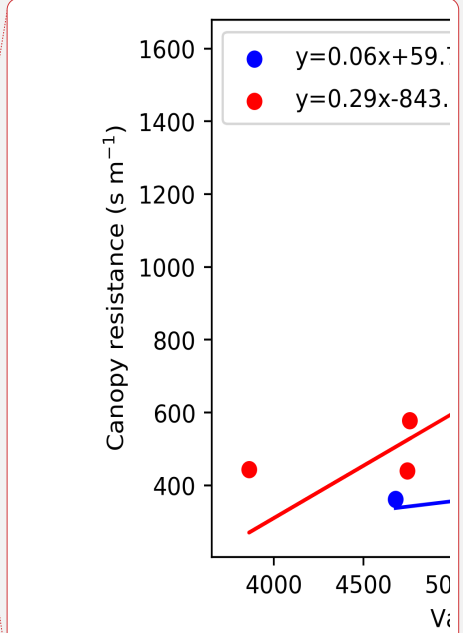
1305

1306

1307

1308

1309



Deleted:

Formatted: Font: (Default) Times New Roman, Font colour: Text 1

Formatted: Font: 11.5 pt

Deleted: and

Formatted: Font colour: Text 1

Formatted: Font colour: Text 1

B12

Appendix A: Table of Abbreviations

Formatted: Font: Bold, Underline, Font colour: Text 1

Formatted: Centred

<u>Name</u>	<u>Abrv. used</u>
-	-
<u>Latent heat flux</u>	<u>LH</u>
<u>Sensible heat flux</u>	<u>SH</u>
<u>Ground heat flux</u>	<u>GH</u>
<u>Evaporative Fraction</u>	<u>EF</u>
<u>2 m air temperature</u>	<u>T_{air}</u>
<u>vapor pressure deficit</u>	<u>VPD</u>
<u>gross primary production</u>	<u>GPP</u>
<u>net radiation</u>	<u>NR</u>
<u>aerosol direct radiative effect</u>	<u>ADRE</u>
<u>aerosol diffuse radiation fertilization effect</u>	<u>ADFE</u>
<u>diffuse radiation</u>	<u>diffuse_{frac}</u>
<u>Santa Barbara discrete ordinates radiative transfer Atmospheric Radiative Transfer Model</u>	<u>SBDART</u>
<u>AErosol RObotic NETwork</u>	<u>AERONET</u>
<u>Volumetric soil water content</u>	<u>VWC</u>
<u>surface temperature</u>	<u>T_{surf}</u>
<u>relative humidity</u>	<u>RH</u>
<u>Aerosol Optical Depth</u>	<u>AOD</u>
<u>Single Scattering Albedo</u>	<u>SSA</u>
<u>High AOD-Low T_{air}</u>	<u>HALT</u>
<u>High AOD-High T_{air}</u>	<u>HAHT</u>
<u>Low AOD- High T_{air}</u>	<u>LAHT</u>
<u>Outgoing long wave radiation at surface</u>	<u>LW_{out}</u>
<u>canopy resistance</u>	<u>r_s</u>
<u>aerodynamic resistance to heat transfer</u>	<u>r_a</u>
<u>Sensible heat fraction</u>	<u>SHE</u>
<u>Latent heat fraction</u>	<u>LHE</u>

Formatted: Subscript

Formatted: Subscript

Formatted: Subscript

Formatted: Font colour: Text 1

Formatted: Subscript

Formatted: Font colour: Text 1

Formatted: Font colour: Text 1

Formatted: Line spacing: 1.5 lines

B13

Page 12: [1] Deleted Microsoft Office User 20/09/2021 17:05:00

Page 12: [1] Deleted Microsoft Office User 20/09/2021 17:05:00

Page 12: [1] Deleted Microsoft Office User 20/09/2021 17:05:00

Page 12: [1] Deleted Microsoft Office User 20/09/2021 17:05:00

Page 12: [1] Deleted Microsoft Office User 20/09/2021 17:05:00

Page 12: [1] Deleted Microsoft Office User 20/09/2021 17:05:00

Page 12: [1] Deleted Microsoft Office User 20/09/2021 17:05:00

Page 12: [1] Deleted Microsoft Office User 20/09/2021 17:05:00

Page 12: [1] Deleted Microsoft Office User 20/09/2021 17:05:00

Page 12: [2] Deleted Microsoft Office User 20/09/2021 17:38:00

Page 12: [2] Deleted Microsoft Office User 20/09/2021 17:38:00

Page 12: [2] Deleted Microsoft Office User 20/09/2021 17:38:00

Page 12: [2] Deleted Microsoft Office User 20/09/2021 17:38:00

Page 12: [2] Deleted Microsoft Office User 20/09/2021 17:38:00

Page 12: [2] Deleted Microsoft Office User 20/09/2021 17:38:00

Page 12: [3] Deleted Microsoft Office User 20/09/2021 17:43:00

Page 12: [3] Deleted Microsoft Office User 20/09/2021 17:43:00

Page 12: [3] Deleted Microsoft Office User 20/09/2021 17:43:00

Page 12: [3] Deleted Microsoft Office User 20/09/2021 17:43:00

Page 12: [3] Deleted Microsoft Office User 20/09/2021 17:43:00

Page 12: [4] Deleted Microsoft Office User 20/09/2021 17:40:00

Page 12: [4] Deleted Microsoft Office User 20/09/2021 17:40:00

Page 12: [4] Deleted Microsoft Office User 20/09/2021 17:40:00

Page 12: [4] Deleted Microsoft Office User 20/09/2021 17:40:00

Page 12: [5] Deleted Microsoft Office User 20/09/2021 17:44:00

Page 12: [5] Deleted Microsoft Office User 20/09/2021 17:44:00

Page 12: [6] Deleted Microsoft Office User 20/09/2021 18:35:00

Page 12: [6] Deleted Microsoft Office User 20/09/2021 18:35:00

Page 12: [6] Deleted Microsoft Office User 20/09/2021 18:35:00

Page 12: [6] Deleted Microsoft Office User 20/09/2021 18:35:00

Page 12: [6] Deleted Microsoft Office User 20/09/2021 18:35:00

Page 12: [6] Deleted Microsoft Office User 20/09/2021 18:35:00

Page 12: [6] Deleted Microsoft Office User 20/09/2021 18:35:00

▲ Page 12: [6] Deleted Microsoft Office User 20/09/2021 18:35:00

▼
▲ Page 12: [6] Deleted Microsoft Office User 20/09/2021 18:35:00

▼
▲ Page 12: [6] Deleted Microsoft Office User 20/09/2021 18:35:00

▼
▲ Page 12: [6] Deleted Microsoft Office User 20/09/2021 18:35:00

▼
▲ Page 12: [6] Deleted Microsoft Office User 20/09/2021 18:35:00

▼
▲ Page 12: [6] Deleted Microsoft Office User 20/09/2021 18:35:00

▼
▲ Page 12: [6] Deleted Microsoft Office User 20/09/2021 18:35:00

▼
▲ Page 12: [6] Deleted Microsoft Office User 20/09/2021 18:35:00

▼
▲ Page 12: [6] Deleted Microsoft Office User 20/09/2021 18:35:00

▼
▲ Page 12: [7] Deleted Microsoft Office User 20/09/2021 21:14:00

▼
▲ Page 12: [7] Deleted Microsoft Office User 20/09/2021 21:14:00

▼
▲ Page 12: [7] Deleted Microsoft Office User 20/09/2021 21:14:00

▼
▲ Page 12: [7] Deleted Microsoft Office User 20/09/2021 21:14:00

▼
▲ Page 12: [7] Deleted Microsoft Office User 20/09/2021 21:14:00

▼
▲ Page 12: [7] Deleted Microsoft Office User 20/09/2021 21:14:00

▼
▲